IEEE Access
Multidisciplinary ⋮ Rapid Review ⋮ Open Access Journal

Received June 7, 2020, accepted June 20, 2020, date of publication June 25, 2020, date of current version July 7, 2020.

Digital Object Identifier 10.1109/ACCESS.2020.3004844

Design for Prespecified Ratios Between Six Energy Peaks Using a Planar Symmetric Dual-Body Vibration System

WOOSEOK RYU, YEONG GEOL LEE, CHUNG GEUN JEON, AND YONG JE CHOI
Department of Mechanical Engineering, Yonsei University, Seoul 03722, South Korea

Corresponding author: Yong Je Choi (yjchoi@yonsei.ac.kr)

This work was supported by the Basic Science Research Program through the National Research Foundation of Korea (NRF) funded by the Ministry of Education under Grant 2018R1D1A1B07048708.

ABSTRACT When the design of a vibration system requires a broad bandwidth, the numbers and the ratios of energy peaks become major design factors. In particular, within a specific range of frequency, an increase in the number of peaks can widen the valid working bandwidth by decreasing the distances between peaks. In this paper, a planar symmetric dual-body vibration system is used to implement desired work ratios at six target frequencies. The geometrical relation between vibration modes and energy peaks is investigated to develop the design method and introduces geometrical representation of vibration modes of a symmetric dual-body system together. Six vibration modes of a symmetric dual-body system are divided into two groups with three vibration modes that represent the centers of vibration. It is shown that the orthocenters of two modal triangles of each of two rigid bodies coincide with its center of mass. The frequency responses to both direct and base excitations are derived in terms of vibration centers and target frequencies, and thus work ratios are obtained. Finally, the derived equation of work ratios is used to determine the modal matrix composed of the vibration modes when the desired mass, specific work ratios, and target resonant frequencies are given. Consequently, the corresponding stiffness matrix is found and realized. Numerical examples of four cases with different work ratios are presented to illustrate the proposed design method.

INDEX TERMS Broad bandwidth, symmetric dual-body vibration system, resonant frequency, vibration mode, work ratio.

I. INTRODUCTION

When designs of vibration systems related to bandwidth such as vibration-based energy harvesters and vibration absorbers, the ratio of the energy peaks at the resonant frequencies has been emphasized as an important design factor because the bandwidth of a vibration system is affected by the magnitudes of the peaks [1]. Accordingly, various design methods and systems have been developed to regulate the peaks of multi-modal systems.

One approach uses a multiple mass array composed of independent one-degree-of-freedom (1-DOF) systems. Since all the vibration modes of the system are decoupled, the peaks can be tuned independently [2], [3]. However, when a pure force (or a pure moment) is applied to the system, unexcited modes such as pure rotational (or pure translational) modes exist, and it can cause unexpected decrease of the effective bandwidth. Thus, Tang and Yang have explained the coupling effect between stacked masses with 1-DOF and developed a multimodal piezoelectric energy harvesting model [4]. A beam system with multiple proof masses was presented for the design of piezoelectric (or electromagnetic) harvesters with widened effective bandwidth [5]. Although these systems improved their performance by extending the effective bandwidth, adjusting to specific energy peaks at the target frequencies was difficult because the relation among coupled vibration modes was uncertain.

For these reasons, the geometrical relation among vibration modes has been investigated and used to design vibration systems. First, Blanchet introduced a geometrical characteristic of vibration modes in a planar single-body vibration system [6]. He showed that the triangle formed by three vibration

The associate editor coordinating the review of this manuscript and approving it for publication was Waleed Ejaz.

centers has a specific configuration in which the orthocenter of the triangle coincides with the center of mass. Dan and Choi interpreted the vibration modes in the three-dimensional space as the axes of vibration and introduced the analytical expressions of the axes of vibration satisfying the geometrical conditions of the planes of symmetry [7]. They have also demonstrated a method on how to eliminate the undesired peaks in the spatial optical pick-up for a spatial system with one plane-of-symmetry [8]. Several design methods for a vibration energy harvester that utilized the above geometrical properties were presented. Kim and Choi developed a design method for a planar single-body vibration system that satisfies the requirement for the prespecified ratio of energy peaks at three target frequencies [1]. This design method was applied to the development of the serial linkage type vibration energy harvesters using polyvinylidene fluoride films and electromagnets [9], [10].

The previous design methods using geometrical properties of the vibration modes have focused on a single-body vibration system in 2D or 3D space. Clearly, the number of peaks of a planar single-body system is limited to three. To increase the number of peaks in this paper, we use a planar vibration system that consists of two rigid bodies connected to each other and supported by a symmetrical spring system. Each of two rigid bodies has six vibration modes, which is used to widen the effective bandwidth of a system within a specific range of frequency. A new design method of a symmetric dual-body system for any prespecified work ratios at the six target frequencies is presented, and numerical examples are illustrated with figures.

This paper is organized as follows: Section II explains the theoretical preliminaries of a symmetric dual-body vibration system. In Section III, the design method of a dual-body system is developed by deriving the stiffness matrix that satisfies the desired parameters, such as target resonant frequencies, desired mass properties, and work ratios. Numerical examples are illustrated in Section IV. Finally, the comparison and discussion of the results are given in Section V.

II. THEORETICAL PRELIMINARIES TO A PLANAR SYMMETRIC DUAL-BODY VIBRATION SYSTEM

A. EQUATION OF MOTION OF A SINGLE-BODY SYSTEM

For undamped free vibration, the equation of motion (EOM) of a single rigid body supported by n line springs (Fig. 1) is given by

$$\boldsymbol{M}\ddot{\hat{\boldsymbol{X}}} + \boldsymbol{K}\hat{\boldsymbol{X}} = \boldsymbol{0}, \tag{1}$$

where $\boldsymbol{M}$ and $\boldsymbol{K}$ are the real 3×3 inertia and stiffness matrices, respectively. The general displacement $\hat{\boldsymbol{X}}$ of the rigid body can be written in terms of a line (bound) vector as

$$\hat{\boldsymbol{X}} = \hat{\boldsymbol{D}}e^{\mathrm{i}\omega t}, \tag{2}$$

where ω denotes the natural frequency of the system. $\hat{\boldsymbol{D}}$ is the time-independent displacement of the rigid body and can be

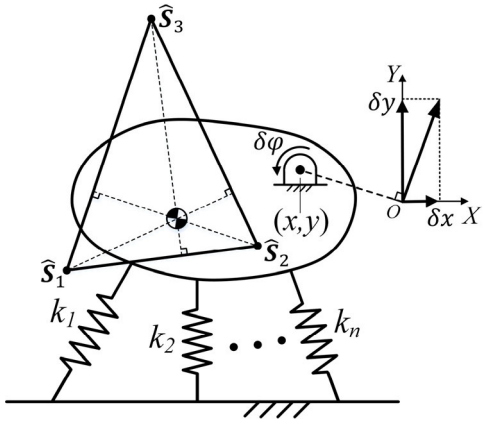

FIGURE 1. General displacements, normal modes and modal triangle of a single-body system.

expressed by

$$\hat{\boldsymbol{D}} = \begin{bmatrix} \delta x & \delta y & \delta\varphi \end{bmatrix}^T, \tag{3}$$

where δx and δy are the x- and y-components of small translational displacement of a point on the rigid body coincident with the origin as shown in Fig. 1. $\delta\varphi$ is the small angular displacement. Dividing $\hat{\boldsymbol{D}}$ by $\delta\varphi$ gives the unit line vector $\hat{\boldsymbol{S}}$ that represents the line parallel to the Z-axis and passing through the instant center of motion at (x, y):

$$\hat{\boldsymbol{S}} = \begin{bmatrix} y & -x & 1 \end{bmatrix}^T. \tag{4}$$

By substituting (2) and (4) into (1), the solutions of (1) are given by three normal modes of vibration and can be expressed in the same form as (4)

$$\hat{\boldsymbol{S}}_P = \begin{bmatrix} y_P & -x_P & 1 \end{bmatrix}^T \quad (P = 1, 2, 3). \tag{5}$$

A modal triangle is defined as a triangle constructed by three points through which the three line vectors $\hat{\boldsymbol{S}}_P$'s pass. It was shown in [6] that the orthogonality of normal modes with respect to the inertia matrix can be geometrically interpreted such that the center of mass coincides with the orthocenter of the modal triangle as shown in Fig. 1. (x_P, y_P) are the coordinates of the vibration center of the Pth normal mode. Normal modes of vibration are orthogonal to each other with respect to the inertia and stiffness matrices, and they can be written as

$$\boldsymbol{S}^T\boldsymbol{M}\boldsymbol{S} = \begin{bmatrix} \tilde{m}_1 & 0 & 0 \\ 0 & \tilde{m}_2 & 0 \\ 0 & 0 & \tilde{m}_3 \end{bmatrix} \quad \text{and}$$
$$\boldsymbol{S}^T\boldsymbol{K}\boldsymbol{S} = \begin{bmatrix} \tilde{k}_1 & 0 & 0 \\ 0 & \tilde{k}_2 & 0 \\ 0 & 0 & \tilde{k}_3 \end{bmatrix}, \tag{6}$$

where $\boldsymbol{S} = \begin{bmatrix} \hat{\boldsymbol{S}}_1 & \hat{\boldsymbol{S}}_2 & \hat{\boldsymbol{S}}_3 \end{bmatrix}$.

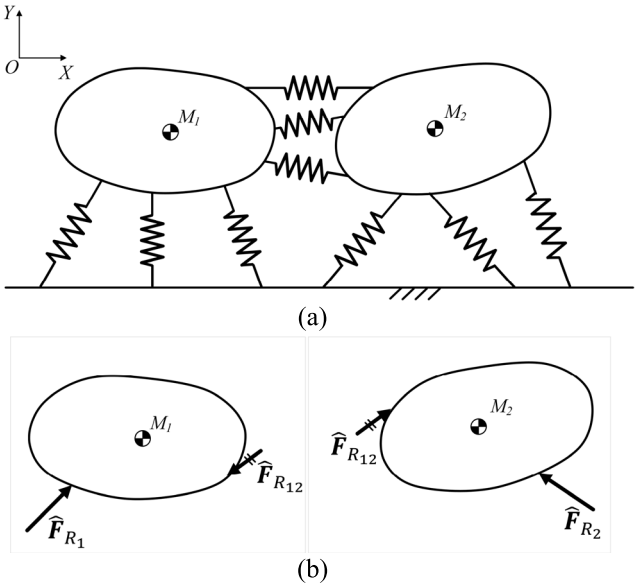

FIGURE 2. (a) Vibration system composed of two rigid bodies and (b) free body diagrams.

B. EQUATION OF MOTION OF A DUAL-BODY SYSTEM

We consider two rigid bodies (M_1 and M_2) that are elastically suspended and connected each other in a plane (Fig. 2(a)) and let $\hat{\boldsymbol{X}}_n$ denote a general displacement of the nth rigid body expressed in terms of a line (bound) vector. The EOMs of two rigid bodies can be written as

$$\boldsymbol{M}_1\ddot{\hat{\boldsymbol{X}}}_1 = -\hat{\boldsymbol{F}}_{R_1} - \hat{\boldsymbol{F}}_{R_{12}} \text{ and } \boldsymbol{M}_2\ddot{\hat{\boldsymbol{X}}}_2 = -\hat{\boldsymbol{F}}_{R_2} + \hat{\boldsymbol{F}}_{R_{12}}, \quad (7)$$

where $\boldsymbol{M}_n$ is the inertia matrix of the nth rigid body.

$\hat{\boldsymbol{F}}_{R_n}$ and $\hat{\boldsymbol{F}}_{R_{12}}$ are the ground reaction force and the reaction force between two rigid bodies, respectively, as shown in Fig. 2(b). The reaction forces are given by

$$\hat{\boldsymbol{F}}_{R_1} = \boldsymbol{K}_1\hat{\boldsymbol{X}}_1, \hat{\boldsymbol{F}}_{R_2} = \boldsymbol{K}_2\hat{\boldsymbol{X}}_2 \text{ and } \hat{\boldsymbol{F}}_{R_{12}} = \boldsymbol{K}_{12}\left(\hat{\boldsymbol{X}}_1 - \hat{\boldsymbol{X}}_2\right), \quad (8)$$

where $\boldsymbol{K}_n (\in R^{3\times3})$ and $\boldsymbol{K}_{12} (\in R^{3\times3})$ are the stiffness matrices corresponding to the springs of the nth rigid body and those connected between two rigid bodies, respectively. Substituting (8) into (7) yields

$$\begin{aligned} &\boldsymbol{M}_1\ddot{\hat{\boldsymbol{X}}}_1 + (\boldsymbol{K}_1 + \boldsymbol{K}_{12})\hat{\boldsymbol{X}}_1 - \boldsymbol{K}_{12}\hat{\boldsymbol{X}}_2 = \boldsymbol{0} \quad \text{and} \\ &\boldsymbol{M}_2\ddot{\hat{\boldsymbol{X}}}_2 + (\boldsymbol{K}_2 + \boldsymbol{K}_{12})\hat{\boldsymbol{X}}_2 - \boldsymbol{K}_{12}\hat{\boldsymbol{X}}_1 = \boldsymbol{0}. \end{aligned} \quad (9)$$

From (9), the EOM for undamped free vibration of a dual-body system can be obtained as

$$\boldsymbol{M}\ddot{\tilde{\boldsymbol{X}}} + \boldsymbol{K}\tilde{\boldsymbol{X}} = \boldsymbol{0}, \quad (10)$$

where $\boldsymbol{M} = \begin{bmatrix} \boldsymbol{M}_1 & \boldsymbol{0}(\in R^{3\times3}) \\ \boldsymbol{0}(\in R^{3\times3}) & \boldsymbol{M}_2 \end{bmatrix} \in R^{6\times6}$ and $\boldsymbol{K} = \begin{bmatrix} \boldsymbol{K}_1 + \boldsymbol{K}_{12} & -\boldsymbol{K}_{12} \\ -\boldsymbol{K}_{12} & \boldsymbol{K}_2 + \boldsymbol{K}_{12} \end{bmatrix} \in R^{6\times6}$. $\tilde{\boldsymbol{X}} \left(= \left[\hat{\boldsymbol{X}}_1^T \ \hat{\boldsymbol{X}}_2^T\right]^T \in R^{6\times1}\right)$ is composed of two line vectors $\hat{\boldsymbol{X}}_1$ and $\hat{\boldsymbol{X}}_2$ and referred here as a line vector chain. The general form of $\tilde{\boldsymbol{X}}$ for free vibration given by (10) is written as

$$\tilde{\boldsymbol{X}} = \begin{bmatrix} \hat{\boldsymbol{X}}_1 \\ \hat{\boldsymbol{X}}_2 \end{bmatrix} = \tilde{\boldsymbol{D}}e^{i\omega t} = \begin{bmatrix} \hat{\boldsymbol{D}}_1 \\ \hat{\boldsymbol{D}}_2 \end{bmatrix} e^{i\omega t}. \quad (11)$$

In (11), $\tilde{\boldsymbol{D}}$ is expressed by

$$\begin{aligned} \tilde{\boldsymbol{D}} &= \begin{bmatrix} \hat{\boldsymbol{D}}_1^T & \hat{\boldsymbol{D}}_2^T \end{bmatrix}^T \\ &= \begin{bmatrix} \delta x_1 & \delta y_1 & \delta\varphi_1 & \delta x_2 & \delta y_2 & \delta\varphi_2 \end{bmatrix}^T. \end{aligned} \quad (12)$$

The general displacements $\tilde{D}$ of a dual-body system are depicted in Fig. 3.

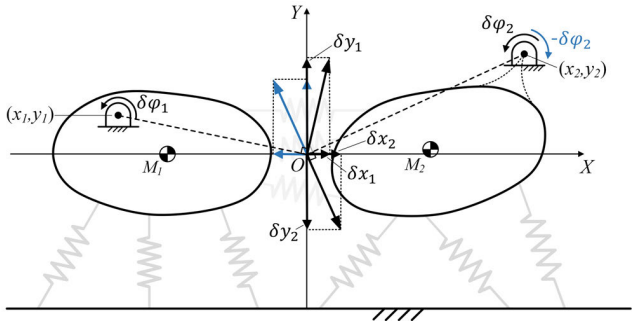

FIGURE 3. General displacements of a planar dual-body system.

(12) can be rewritten in a normalized form as

$$\tilde{\boldsymbol{D}} = \begin{bmatrix} \delta\varphi_1\hat{\boldsymbol{S}}_1^T & \delta\varphi_2\hat{\boldsymbol{S}}_2^T \end{bmatrix}^T, \quad (13)$$

where the line vector chain $\tilde{\boldsymbol{D}}$ represents the rotational motions of two rigid bodies about the instantaneous centers with the ratio between two small angular displacements ($\delta\varphi_1 : \delta\varphi_2$). The signs of $\delta\varphi_1$ and $\delta\varphi_2$ mean the phase difference in motions (Fig. 3). If the signs are identical, the motions of two rigid bodies are in phase. Otherwise, the two motions are 180 ° out of phase.

By substituting (11) into (10), we obtain the time invariant form of (10) as

$$\left(\boldsymbol{K} - \omega^2\boldsymbol{M}\right)\tilde{\boldsymbol{D}} = \boldsymbol{0}. \quad (14)$$

For a non-trivial solution of $\tilde{\boldsymbol{D}}$, ω_j^2 and $\tilde{\boldsymbol{D}}_j \left(= \left[\hat{\boldsymbol{D}}_{1,j}^T \ \hat{\boldsymbol{D}}_{2,j}^T\right]^T\right)$ can be viewed as the eigenvalue (natural frequency) and the corresponding eigenvector (mode shape) of $\boldsymbol{M}^{-1}\boldsymbol{K} \left(\in R^{6\times6}\right)$, respectively. In general, the number of natural frequencies j is decided by the rank of $\boldsymbol{M}^{-1}\boldsymbol{K}$. If the matrix $\boldsymbol{M}^{-1}\boldsymbol{K}$ of a dual-body system has full rank, the system has six natural frequencies. It can be expressed by $j = 3n$ for the number of rigid bodies n. The line vector $\hat{\boldsymbol{D}}_{n,j}$ of $\tilde{\boldsymbol{D}}$ is the vibration mode of the nth rigid body corresponding to ω_j. Thus, a dual-body system has a total of 12 vibration modes and they exist in pairs, i.e., $\hat{\boldsymbol{D}}_{1,j}$ and $\hat{\boldsymbol{D}}_{2,j}$ at ω_j, because motions of two rigid bodies interact with each other through the connected springs.

C. VIBRATION MODES OF A SYMMETRIC DUAL-BODY SYSTEM

The jth vibration mode of a dual-body system of (13) can be written as

$$\tilde{\boldsymbol{D}}_j = \begin{bmatrix} \hat{\boldsymbol{D}}_{1,j}^T & \hat{\boldsymbol{D}}_{2,j}^T \end{bmatrix}^T = \begin{bmatrix} \delta\varphi_{1,j}\hat{\boldsymbol{S}}_{1,j}^T & \delta\varphi_{2,j}\hat{\boldsymbol{S}}_{2,j}^T \end{bmatrix}^T. \quad (15)$$

The twelve normal modes of a dual-body system are illustrated in Fig. 4(a).

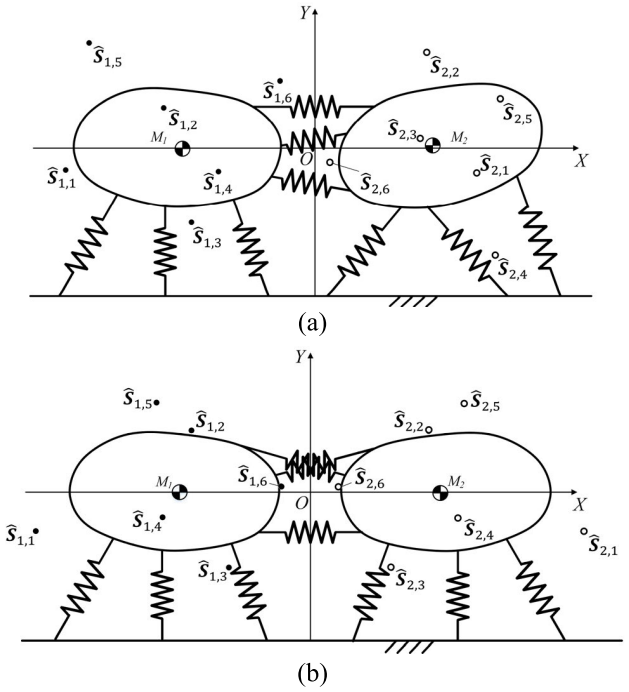

FIGURE 4. Normal modes $\hat{\boldsymbol{S}}_{n,j}$ of (a) general dual-body system and (b) symmetric dual-body system.

If two rigid bodies of a dual-body system have identical stiffnesses and mass properties (including the masses, moments of inertias, and the locations of mass centers) and the geometric shape is symmetrical about the Y-axis (Fig. 4(b)), the normal modes of each of two rigid bodies are located symmetrically. Furthermore, the magnitudes of two small rotational displacements are equal, i.e., $\|\delta\varphi_1\| = \|\delta\varphi_2\|$. The verification of these properties of a symmetric dual-body system is given in Appendix A. Since the vibration modes of each of two rigid bodies are symmetric about the Y-axis, using two configurations derived in Appendix A, $\tilde{\boldsymbol{D}}_j$ of (15) can be rewritten in the normalized form as

$$\begin{aligned} \tilde{\boldsymbol{D}}_j &= \begin{bmatrix} \hat{\boldsymbol{S}}_{1,j}^T & \hat{\boldsymbol{S}}_{2,j}^T \end{bmatrix}^T \\ &= \begin{bmatrix} y_{1,j} & -x_{1,j} & 1 & y_{1,j} & x_{1,j} & 1 \end{bmatrix}^T \quad \text{or} \quad (16\text{-}1) \\ &= \begin{bmatrix} y_{1,j} & -x_{1,j} & 1 & -y_{1,j} & -x_{1,j} & -1 \end{bmatrix}^T. \end{aligned} \quad (16\text{-}2)$$

D. ORTHOGONALITY OF A SYMMETRIC DUAL-BODY SYSTEM

The modal matrix $\boldsymbol{S}$ can be formed using $\tilde{\boldsymbol{D}}_j (j = 1, \cdots, 6)$ as column vectors such that

$$\boldsymbol{S} = \begin{bmatrix} \hat{\boldsymbol{S}}_{1,1} & \hat{\boldsymbol{S}}_{1,2} & \hat{\boldsymbol{S}}_{1,3} & \hat{\boldsymbol{S}}_{1,4} & \hat{\boldsymbol{S}}_{1,5} & \hat{\boldsymbol{S}}_{1,6} \\ \hat{\boldsymbol{S}}_{2,1} & \hat{\boldsymbol{S}}_{2,2} & \hat{\boldsymbol{S}}_{2,3} & \hat{\boldsymbol{S}}_{2,4} & \hat{\boldsymbol{S}}_{2,5} & \hat{\boldsymbol{S}}_{2,6} \end{bmatrix} \in R^{6\times 6}. \quad (17)$$

The inertia and stiffness matrices can be diagonalized using the modal matrix $\boldsymbol{S}$

$$\begin{aligned} \boldsymbol{S}^T\boldsymbol{M}\boldsymbol{S} &= \begin{bmatrix} \boldsymbol{A}_1 & \boldsymbol{0} \\ \boldsymbol{0} & \boldsymbol{A}_2 \end{bmatrix} \\ &= \begin{bmatrix} \tilde{m}_1 & 0 & 0 & & & \\ 0 & \tilde{m}_2 & 0 & & \boldsymbol{0}(\in R^{3\times 3}) & \\ 0 & 0 & \tilde{m}_3 & & & \\ & & & \tilde{m}_4 & 0 & 0 \\ & \boldsymbol{0}(\in R^{3\times 3}) & & 0 & \tilde{m}_5 & 0 \\ & & & 0 & 0 & \tilde{m}_6 \end{bmatrix} \quad \text{and} \end{aligned} \quad (18\text{-}1)$$

$$\begin{aligned} \boldsymbol{S}^T\boldsymbol{K}\boldsymbol{S} &= \begin{bmatrix} \boldsymbol{B}_1 & \boldsymbol{0} \\ \boldsymbol{0} & \boldsymbol{B}_2 \end{bmatrix} \\ &= \begin{bmatrix} \tilde{k}_1 & 0 & 0 & & & \\ 0 & \tilde{k}_2 & 0 & & \boldsymbol{0}(\in R^{3\times 3}) & \\ 0 & 0 & \tilde{k}_3 & & & \\ & & & \tilde{k}_4 & 0 & 0 \\ & \boldsymbol{0}(\in R^{3\times 3}) & & 0 & \tilde{k}_5 & 0 \\ & & & 0 & 0 & \tilde{k}_6 \end{bmatrix}. \end{aligned} \quad (18\text{-}2)$$

In a symmetric dual-body system, two conditions to satisfy (18-1) are examined.

First, all the off-diagonal elements of $\boldsymbol{A}_1$ and $\boldsymbol{A}_2$ in (18-1) become zeros due to the orthogonality of the vibration modes and can be expressed by

$$\begin{aligned} &\hat{\boldsymbol{S}}_{1,P}^T\boldsymbol{M}_1\hat{\boldsymbol{S}}_{1,Q} + \hat{\boldsymbol{S}}_{2,P}^T\boldsymbol{M}_2\hat{\boldsymbol{S}}_{2,Q} = 0 \\ &\qquad (P, Q = 1, 2, 3 \quad \text{and } P \neq Q) \text{ and} \end{aligned} \quad (19\text{-}1)$$

$$\begin{aligned} &\hat{\boldsymbol{S}}_{1,V}^T\boldsymbol{M}_1\hat{\boldsymbol{S}}_{1,W} + \hat{\boldsymbol{S}}_{2,V}^T\boldsymbol{M}_2\hat{\boldsymbol{S}}_{2,W} = 0 \\ &\qquad (V, W = 4, 5, 6 \quad \text{and } V \neq W). \end{aligned} \quad (19\text{-}2)$$

If we substitute (16-1) (or (16-2)) and (A1) into (19-1) and (19-2), we obtain the following relations from the off-diagonal elements of $\boldsymbol{A}_1$ and $\boldsymbol{A}_2$ of (18-1):

$$\begin{aligned} &\hat{\boldsymbol{S}}_{1,P}^T\boldsymbol{M}_1\hat{\boldsymbol{S}}_{1,Q} = \hat{\boldsymbol{S}}_{2,P}^T\boldsymbol{M}_2\hat{\boldsymbol{S}}_{2,Q} = \Delta_1 \quad \text{and} \\ &\hat{\boldsymbol{S}}_{1,V}^T\boldsymbol{M}_1\hat{\boldsymbol{S}}_{1,W} = \hat{\boldsymbol{S}}_{2,V}^T\boldsymbol{M}_2\hat{\boldsymbol{S}}_{2,W} = \Delta_2, \end{aligned} \quad (20)$$

where $\Delta_1 = (c - x_{1,P})(c - x_{1,Q}) + y_{1,P}y_{1,Q} + G$, $\Delta_2 = (c - x_{1,V})(c - x_{1,W}) + y_{1,V}y_{1,W} + G$, $G = \frac{I}{m}$ and c is the distance between the mass center of each rigid body and the origin. Clearly, Δ_1 and Δ_2 should be zeros when (19-1) holds. It means that the six normal modes of each rigid body are divided into two groups each of which contains three normal modes satisfying (19-1) and (19-2). Three normal

modes of each group are also orthogonal to each other with respect to the inertia matrix $\boldsymbol{M}_n$. Geometrically, the orthocenter of the modal triangle constructed by three modes of each group coincides with the center of each mass (Fig. 5). Now, the matrices composed of three vibration modes, which are divided into two groups in the nth rigid body, are defined as $\boldsymbol{S}_{n,1}(\in R^{3\times 3})$ and $\boldsymbol{S}_{n,2}(\in R^{3\times 3})$, respectively. The triangles associated with $\boldsymbol{S}_{n,1}$ and $\boldsymbol{S}_{n,2}$ are called modal triangles of a symmetric dual-body system, which are depicted by blue and red triangles in Fig. 5. Now, the modal matrix of (17) can be rewritten as

$$\boldsymbol{S} = \begin{bmatrix} \boldsymbol{S}_{1,1} & \boldsymbol{S}_{1,2} \\ \boldsymbol{S}_{2,1} & \boldsymbol{S}_{2,2} \end{bmatrix}. \tag{21}$$

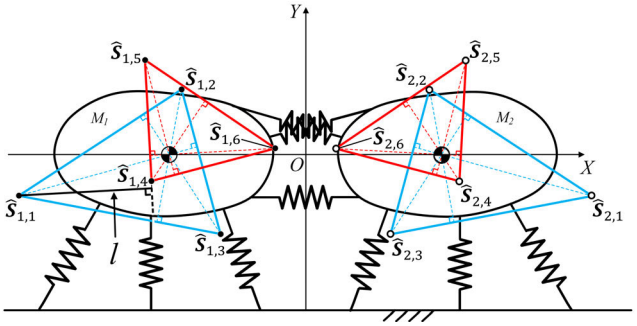

FIGURE 5. Geometrical configuration of six normal modes in symmetric dual-body system and modal triangles (blue and red triangles).

Second, all the elements of the 3×3 upper right and lower left sub-matrices in (18-1) should be zeros, and thus we have

$$\hat{\boldsymbol{S}}^T_{1,P(orV)}\boldsymbol{M}_1\hat{\boldsymbol{S}}_{1,V(or\ P)} + \hat{\boldsymbol{S}}^T_{2,P(orV)}\boldsymbol{M}_2\hat{\boldsymbol{S}}_{2,V(or\ P)} = 0 \quad (P = 1, 2, 3 \quad \text{and } V = 4, 5, 6). \tag{22}$$

Each term on the left side of (22) means the distance between each side of one modal triangle and the corresponding vertex of the other modal triangle of the nth rigid body (e.g., l in Fig. 5). Since the vibration centers of two rigid bodies are located symmetrically, the two distances corresponding to each pair of two rigid bodies are identical. Therefore, the vibration modes of one of two groups should be 180 ° out of phase to satisfy (22). In other words, the vibration modes of one group are in phase and those of the other group are 180 ° out of phase, which can be expressed by (16-1) and (16-2), respectively. The instantaneous motions of two rigid bodies are illustrated in Fig. 6. Figs. 6(a) and 6(b) depict the motions of two rigid bodies being in phase and 180 ° out of phase, respectively.

If the inertia and stiffness matrices are given, the phases between the vibration modes are determined. Otherwise, from the two conditions explained above, the modal matrix of (21) can be represented by one of the following four types:

$$\textbf{TYPE I}: \boldsymbol{S} = \begin{bmatrix} -\boldsymbol{S}_{1,1} & \boldsymbol{S}_{1,2} \\ \boldsymbol{S}_{2,1} & \boldsymbol{S}_{2,2} \end{bmatrix},$$
$$\textbf{TYPE II}: \boldsymbol{S} = \begin{bmatrix} \boldsymbol{S}_{1,1} & -\boldsymbol{S}_{1,2} \\ \boldsymbol{S}_{2,1} & \boldsymbol{S}_{2,2} \end{bmatrix},$$

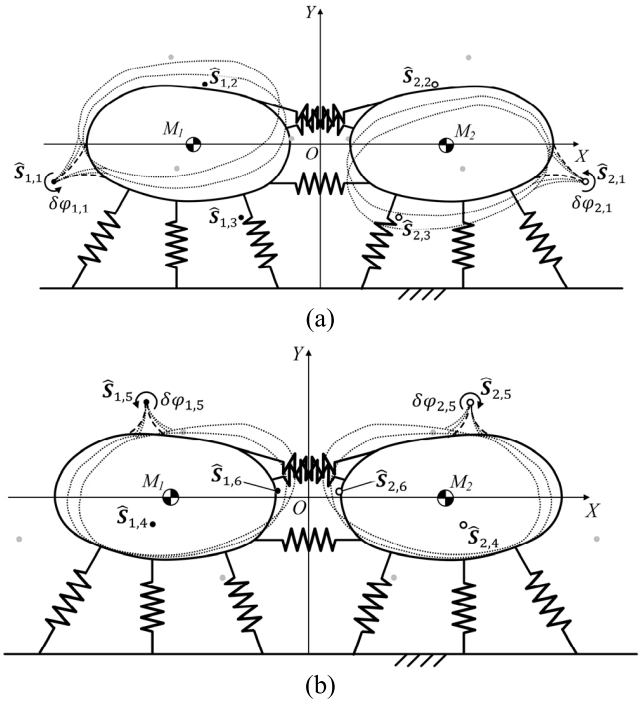

FIGURE 6. Instantaneous motions of two rigid bodies (a) in phase and (b) 180 ° out of phase.

$$\textbf{TYPE III}: \boldsymbol{S} = \begin{bmatrix} \boldsymbol{S}_{1,1} & \boldsymbol{S}_{1,2} \\ -\boldsymbol{S}_{2,1} & \boldsymbol{S}_{2,2} \end{bmatrix} \quad \text{and}$$
$$\textbf{TYPE IV}: \boldsymbol{S} = \begin{bmatrix} \boldsymbol{S}_{1,1} & \boldsymbol{S}_{1,2} \\ \boldsymbol{S}_{2,1} & -\boldsymbol{S}_{2,2} \end{bmatrix} \tag{23}$$

We decided to use **TYPE IV** in this paper, thus $\boldsymbol{S}_{n,1}$ and $\boldsymbol{S}_{n,2}$ are rewritten in terms of $(x_{1,j}, y_{1,j})$ as:

$$\boldsymbol{S}_{1,1} = \begin{bmatrix} y_{1,1} & y_{1,2} & y_{1,3} \\ -x_{1,1} & -x_{1,2} & -x_{1,3} \\ 1 & 1 & 1 \end{bmatrix},$$
$$\boldsymbol{S}_{1,2} = \begin{bmatrix} y_{1,4} & y_{1,5} & y_{1,6} \\ -x_{1,4} & -x_{1,5} & -x_{1,6} \\ 1 & 1 & 1 \end{bmatrix},$$
$$\boldsymbol{S}_{2,1} = \begin{bmatrix} y_{1,1} & y_{1,2} & y_{1,3} \\ x_{1,1} & x_{1,2} & x_{1,3} \\ 1 & 1 & 1 \end{bmatrix} \quad \text{and}$$
$$-\boldsymbol{S}_{2,2} = -\begin{bmatrix} y_{1,4} & y_{1,5} & y_{1,6} \\ x_{1,4} & x_{1,5} & x_{1,6} \\ 1 & 1 & 1 \end{bmatrix}. \tag{24}$$

E. FREQUENCY RESPONSE

1) DIRECT EXCITATION SYSTEM

When a symmetric dual-body system is excited by externally applied harmonic forces $\boldsymbol{F}_1$ and $\boldsymbol{F}_2$ (Fig. 7), the EOM can be expressed by

$$\boldsymbol{M}\ddot{\tilde{\boldsymbol{X}}} + \boldsymbol{C}\dot{\tilde{\boldsymbol{X}}} + \boldsymbol{K}\tilde{\boldsymbol{X}} = \tilde{\boldsymbol{F}}, \tag{25}$$

where $\tilde{\boldsymbol{F}} = \begin{bmatrix} \boldsymbol{F}_1^T & \boldsymbol{F}_2^T \end{bmatrix}^T$ and $\boldsymbol{C}$ is the damping matrix.

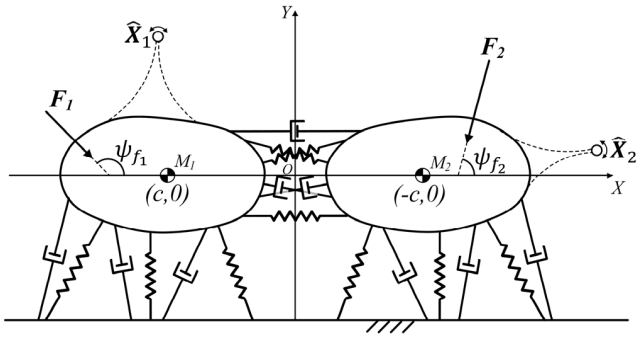

FIGURE 7. Direct force excitation system.

Here, the damping matrix $\boldsymbol{C}$ is assumed that it can be diagonalized by use of the modal matrix $\boldsymbol{S}$ as

$$\left[\tilde{c}\right] = \boldsymbol{S}^T \boldsymbol{C}\boldsymbol{S}, \tag{26}$$

where $\left[\tilde{c}\right] = diag(\tilde{c}_1, \tilde{c}_2, \tilde{c}_3, \tilde{c}_4, \tilde{c}_5, \tilde{c}_6)$ and $\tilde{c}_j = \tilde{\boldsymbol{D}}_j^T \boldsymbol{C}\tilde{\boldsymbol{D}}_j$. The external harmonic forces are given by

$$\tilde{F} = \begin{bmatrix} f_1 \hat{\boldsymbol{s}}_{f_1} e^{i\Omega_1 t} \\ f_2 \hat{\boldsymbol{s}}_{f_2} e^{i\Omega_2 t} \end{bmatrix}, \tag{27}$$

where f_n is the intensity of the force and Ω_n is the driving frequency. $\hat{\boldsymbol{s}}_{f_n}$ is the line of action of the nth force expressed in (Plücker's) ray coordinates:

$$\hat{\boldsymbol{s}}_{f_1} = \begin{bmatrix} C_{\psi_{f_1}} S_{\psi_{f_1}} d_{s_{f_1}} \end{bmatrix}^T \quad \text{and } \hat{\boldsymbol{s}}_{f_2} = \begin{bmatrix} C_{\psi_{f_2}} S_{\psi_{f_2}} d_{s_{f_2}} \end{bmatrix}^T, \tag{28}$$

where the symbols C and S are used to denote the *cosine* and *sine* of the angles, respectively. ψ_{f_n} is the angle between the X-axis and the line of action of the force. $d_{s_{f_n}}$ is the distance between the origin and the line of action. If two external forces are applied at the same driving frequency, i.e., $\Omega_1 = \Omega_2 = \Omega$, the time invariant form of (25) is written as

$$\left(\boldsymbol{K} - \Omega^2 \boldsymbol{M} + i\Omega \boldsymbol{C}\right) \tilde{\boldsymbol{D}} = \begin{bmatrix} f_1 \hat{\boldsymbol{s}}_{f_1} \\ f_2 \hat{\boldsymbol{s}}_{f_2} \end{bmatrix}. \tag{29}$$

$\tilde{\boldsymbol{D}}$ of (29) can be expressed by the linear combination of the normal modes

$$\tilde{\boldsymbol{D}} = \boldsymbol{S}\boldsymbol{v}, \tag{30}$$

where $\boldsymbol{v} = \begin{bmatrix} v_1 & v_2 & v_3 & v_4 & v_5 & v_6 \end{bmatrix}^T \in R^{6\times 1}$ is a constant vector. Substituting (30) into (29) and premultiplying both sides of (29) by $\boldsymbol{S}^T$ yields

$$\begin{bmatrix} \boldsymbol{H}_1 & \boldsymbol{0}(\in R^{3\times 3}) \\ \boldsymbol{0}(\in R^{3\times 3}) & \boldsymbol{H}_2 \end{bmatrix} \boldsymbol{v} = \begin{bmatrix} f_1 \hat{\boldsymbol{S}}_{1,1}^T \hat{\boldsymbol{s}}_{f_1} + f_2 \hat{\boldsymbol{S}}_{2,1}^T \hat{\boldsymbol{s}}_{f_2} \\ \vdots \\ f_1 \hat{\boldsymbol{S}}_{1,6}^T \hat{\boldsymbol{s}}_{f_1} + f_2 \hat{\boldsymbol{S}}_{2,6}^T \hat{\boldsymbol{s}}_{f_2} \end{bmatrix}, \tag{31}$$

where $\boldsymbol{H}_1$ and $\boldsymbol{H}_2$, as shown at the bottom of the page. From (30) and (31), the frequency response can be expressed by

$$\tilde{\boldsymbol{D}} = \begin{bmatrix} \hat{\boldsymbol{D}}_1 \\ \hat{\boldsymbol{D}}_2 \end{bmatrix} = \begin{bmatrix} \sum_{j=1}^{6} v_j \hat{\boldsymbol{S}}_{1,j} \\ \sum_{j=1}^{6} v_j \hat{\boldsymbol{S}}_{2,j} \end{bmatrix}, \tag{32}$$

where $v_j = \frac{f_1 \hat{\boldsymbol{S}}_{1,j}^T \hat{\boldsymbol{s}}_{f_1} + f_2 \hat{\boldsymbol{S}}_{2,j}^T \hat{\boldsymbol{s}}_{f_2}}{\left(\tilde{k}_j - \Omega^2 \tilde{m}_j\right) + i\Omega \tilde{c}_j}$. If the damping ratio $\zeta_j \left(= \frac{\tilde{c}_j}{2\tilde{m}_j \Omega_j}\right)$ is not greater than 0.05, the damping can be considered the light damping. In this case, the resonant frequencies can be regarded as the natural frequencies [12]. Therefore, the jth term of (32) is dominant at the jth resonant frequency (Ω_j). The frequency response at Ω_j can be approximated as

$$\tilde{\boldsymbol{D}}_j = \begin{bmatrix} \hat{\boldsymbol{D}}_{1,j} \\ \hat{\boldsymbol{D}}_{2,j} \end{bmatrix} = \begin{bmatrix} v_j \hat{\boldsymbol{S}}_{1,j} \approx \dfrac{f_1 \hat{\boldsymbol{S}}_{1,j}^T \hat{\boldsymbol{s}}_{f_1} + f_2 \hat{\boldsymbol{S}}_{2,j}^T \hat{\boldsymbol{s}}_{f_2}}{i\Omega_j \tilde{c}_j} \hat{\boldsymbol{S}}_{1,j} \\ v_j \hat{\boldsymbol{S}}_{2,j} \approx \dfrac{f_1 \hat{\boldsymbol{S}}_{1,j}^T \hat{\boldsymbol{s}}_{f_1} + f_2 \hat{\boldsymbol{S}}_{2,j}^T \hat{\boldsymbol{s}}_{f_2}}{i\Omega_j \tilde{c}_j} \hat{\boldsymbol{S}}_{2,j} \end{bmatrix}. \tag{33}$$

The work produced by the external forces at the jth frequency is obtained as

$$\begin{aligned} W_j &= \begin{bmatrix} f_1 \hat{\boldsymbol{s}}_{f_1}^T & f_2 \hat{\boldsymbol{s}}_{f_2}^T \end{bmatrix} \begin{bmatrix} \hat{\boldsymbol{D}}_{1,j} \\ \hat{\boldsymbol{D}}_{2,j} \end{bmatrix} \\ &= v_j \left(f_1 \hat{\boldsymbol{s}}_{f_1}^T \hat{\boldsymbol{S}}_{1,j} + f_2 \hat{\boldsymbol{s}}_{f_2}^T \hat{\boldsymbol{S}}_{2,j} \right) = \frac{\left(f_1 \hat{\boldsymbol{S}}_{1,j}^T \hat{\boldsymbol{s}}_{f_1} + f_2 \hat{\boldsymbol{S}}_{2,j}^T \hat{\boldsymbol{s}}_{f_2} \right)^2}{i\Omega_j \tilde{c}_j}. \end{aligned} \tag{34}$$

In addition, substituting (23) and (28) into (34) yields as (35), shown at the bottom of the page, where the positive and the negative signs of the plus–minus sign ($\pm$) are used for $j = 1, 2, 3$ and $j = 4, 5, 6$, respectively.

$$\boldsymbol{H}_1 = \begin{bmatrix} \tilde{k}_1 - \Omega^2 \tilde{m}_1 + i\Omega \tilde{c}_1 & 0 & 0 \\ 0 & \tilde{k}_2 - \Omega^2 \tilde{m}_2 + i\Omega \tilde{c}_2 & 0 \\ 0 & 0 & \tilde{k}_3 - \Omega^2 \tilde{m}_3 + i\Omega \tilde{c}_3 \end{bmatrix} \quad \text{and}$$

$$\boldsymbol{H}_2 = \begin{bmatrix} \tilde{k}_4 - \Omega^2 \tilde{m}_4 + i\Omega \tilde{c}_4 & 0 & 0 \\ 0 & \tilde{k}_5 - \Omega^2 \tilde{m}_5 + i\Omega \tilde{c}_5 & 0 \\ 0 & 0 & \tilde{k}_6 - \Omega^2 \tilde{m}_6 + i\Omega \tilde{c}_6 \end{bmatrix}.$$

$$W_j = \frac{\left\{ f_1 \left(y_{1,j} C_{\psi_{f_1}} - x_{1,j} S_{\psi_{f_1}} + d_{s_{f_1}} \right) \pm f_2 \left(y_{1,j} C_{\psi_{f_2}} + x_{1,j} S_{\psi_{f_2}} + d_{s_{f_2}} \right) \right\}^2}{2\tilde{m}_j \Omega_j^2 \zeta_j}, \tag{35}$$

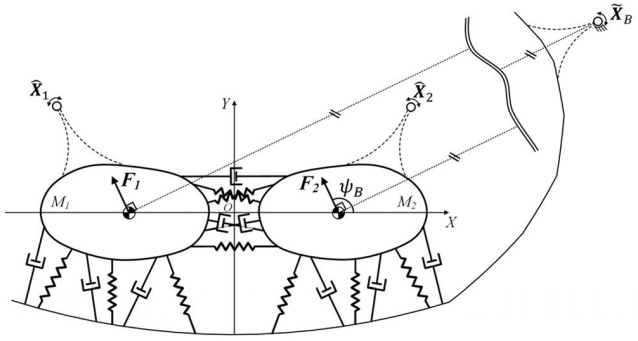

FIGURE 8. Base excitation system.

2) BASE EXCITATION SYSTEM

The base excitation system means a vibration system under base excitation as shown in Fig. 8. The EOM for a base excitation system (Fig. 8) can be written as

$$\boldsymbol{M}\ddot{\tilde{\boldsymbol{X}}} + \boldsymbol{C}\dot{\tilde{\boldsymbol{X}}} + \boldsymbol{K}\tilde{\boldsymbol{X}} = \boldsymbol{C}\dot{\tilde{\boldsymbol{X}}}_B + \boldsymbol{K}\tilde{\boldsymbol{X}}_B, \tag{36}$$

where $\tilde{\boldsymbol{X}}_B$ denotes the displacement of the base. If $\tilde{\boldsymbol{Z}} = \tilde{\boldsymbol{X}} - \tilde{\boldsymbol{X}}_B$, (36) can be rewritten as

$$\boldsymbol{M}\ddot{\tilde{\boldsymbol{Z}}} + \boldsymbol{C}\dot{\tilde{\boldsymbol{Z}}} + \boldsymbol{K}\tilde{\boldsymbol{Z}} = -\boldsymbol{M}\ddot{\tilde{\boldsymbol{X}}}_B. \tag{37}$$

Since the two driving frequencies of the applied forces are identical, the time-independent form of (37) can be expressed by

$$\left(\boldsymbol{K} - \Omega^2\boldsymbol{M} + \mathrm{i}\Omega\boldsymbol{C}\right)\tilde{\boldsymbol{Z}} = \Omega^2\boldsymbol{M}\tilde{\boldsymbol{D}}_B, \tag{38}$$

where $\tilde{\boldsymbol{D}}_B = \varphi_B\left[\, C_{\psi_B}\ S_{\psi_B}\ 0\ \ C_{\psi_B}\ S_{\psi_B}\ 0\,\right]^T$, which is the input displacement of base excitation given by a repetitive translational motions. The external forces in (38) can be written as

$$\tilde{\boldsymbol{F}}\left(=\Omega^2\boldsymbol{M}\tilde{\boldsymbol{D}}_B\right) = \begin{bmatrix} f_1\hat{\boldsymbol{s}}_{f_1} \\ f_2\hat{\boldsymbol{s}}_{f_2} \end{bmatrix}, \tag{39}$$

where $f_1 = f_2 = m\Omega^2\varphi_B$, $\hat{\boldsymbol{s}}_{f_1} = \left[\, C_{\psi_B}\ S_{\psi_B}\ cS_{\psi_B}\,\right]^T$ and $\hat{\boldsymbol{s}}_{f_2} = \left[\, C_{\psi_B}\ S_{\psi_B}\ -cS_{\psi_B}\,\right]^T$. ψ_B is the angle between the X-axis and the line of action of the force produced by base excitation (Fig. 8). In (39), the magnitudes of external forces are proportional to Ω^2 because the input displacement (φ_B) of base excitation remains constant at all the driving frequencies. In a practical design of a base excitation system, the input acceleration due to base excitation is assumed to stay the same. Accordingly, the exerted force is considered constant, i.e., $f_1 = f_2 \equiv f_B$. In this case, the work produced by base excitation at the jth frequency can be obtained from (34)

$$W_j = f_B\begin{bmatrix} \hat{\boldsymbol{s}}_{f_1}^T & \hat{\boldsymbol{s}}_{f_2}^T \end{bmatrix}\tilde{\boldsymbol{Z}}_j = \frac{f_B^2\left(\hat{\boldsymbol{S}}_{1,j}^T\hat{\boldsymbol{s}}_{f_1} + \hat{\boldsymbol{S}}_{2,j}^T\hat{\boldsymbol{s}}_{f_2}\right)^2}{\mathrm{i}\Omega_j\tilde{c}_j}. \tag{40}$$

In addition, substituting (23) and $\hat{\boldsymbol{s}}_{f_n}$ of (39) into (40) yields

$$W_P = \frac{f_B^2\left(2C_{\psi_B}y_{1,P}\right)^2}{2\tilde{m}_P\Omega_P^2\zeta_P}\ (P = 1, 2, 3) \quad \text{and} \tag{41-1}$$

$$W_V = \frac{f_B^2\left(2S_{\psi_B}(-x_{1,V} + c)\right)^2}{2\tilde{m}_V\Omega_V^2\zeta_V}\quad (V = 4, 5, 6). \tag{41-2}$$

Close observations on (41-1) and (41-2) reveal the following findings:

1. When $0° < \psi_B < 90°$, both (41-1) and (41-2) are not zeros. Therefore, the system will have six energy peaks at the resonant frequencies. Moreover, W_P is expressed in terms of $y_{1,P}$, and W_V is given by $x_{1,V}$ and c.
2. When $\psi_B = 0°$, W_V's for $(V = 4, 5, 6)$ of (41-2) become zero . Therefore, the frequency response will show three energy peaks related to three vibration modes of $\boldsymbol{S}_{n,1}$.
3. When $\psi_B = 90°$, W_P's for $(P = 1, 2, 3)$ of (41-1) become zero . Therefore, the frequency response of work will have three energy peaks associated with three vibration modes of $\boldsymbol{S}_{n,2}$.

If $0° < \psi_B < 90°$, the work ratios can be determined from (41-1) and (41-2):

$$1 : \gamma_1 : \gamma_2 = 1 : \frac{\tilde{m}_1\zeta_1\Omega_1^2y_{1,2}^2}{\tilde{m}_2\zeta_2\Omega_2^2y_{1,1}^2} : \frac{\tilde{m}_1\zeta_1\Omega_1^2y_{1,3}^2}{\tilde{m}_3\zeta_3\Omega_3^2y_{1,1}^2} \quad \text{and} \tag{42-1}$$

$$1 : \gamma_4' : \gamma_5' = 1 : \frac{\tilde{m}_4\zeta_4\Omega_4^2\left(-x_{1,5}+c\right)^2}{\tilde{m}_5\zeta_5\Omega_5^2\left(-x_{1,4}+c\right)^2} : \frac{\tilde{m}_4\zeta_4\Omega_4^2\left(-x_{1,6}+c\right)^2}{\tilde{m}_6\zeta_6\Omega_6^2\left(-x_{1,4}+c\right)^2}. \tag{42-2}$$

where $\gamma_1 = \frac{W_2}{W_1}$, $\gamma_2 = \frac{W_3}{W_1}$, $\gamma_4' = \frac{W_5}{W_4}$, and $\gamma_5' = \frac{W_6}{W_4}$. If the desired work ratio $(1 : \gamma_1 : \gamma_2 : \gamma_3 : \gamma_4 : \gamma_5)$ is given, γ_4' and γ_5' correspond to $\frac{\gamma_4}{\gamma_3}$ and $\frac{\gamma_5}{\gamma_3}$, respectively. Using (41-1) and (41-2), $\gamma_3\left(=\frac{W_4}{W_1}\right)$ is found as

$$\gamma_3 = \kappa tan^2\psi_B, \tag{43}$$

where $\kappa = \frac{\tilde{m}_1\Omega_1^2\left(-x_{1,4}+c\right)^2}{\tilde{m}_4\Omega_4^2y_{1,1}^2}$. Consequently, ψ_B is determined as

$$\psi_B = tan^{-1}\left(\sqrt{\frac{\gamma_3}{\kappa}}\right)\quad (0° < \psi_B < 90°). \tag{44}$$

F. GEOMETRIC CONFIGURATION OF K_{12}

Since the derived stiffness matrix to be realized by means of linear springs should be positive definite, we consider only the stiffness matrices with full rank. In this case, the geometric configuration of the spring connections ($\boldsymbol{K}_{12}$) between two rigid bodies can be represented as shown in Fig. 9. The following three cases are not considered in this study because $\boldsymbol{K}_{12}$ is not full rank: 1) three springs meet at a common point, 2) they are parallel to the X-axis, and 3) they are parallel to the Y-axis.

Referring to Fig. 9, when the second spring ($k_{12,2}$) is parallel to the X-axis and the first ($k_{12,1}$) and third ($k_{12,3}$) springs are symmetric about the Y-axis in all cases, $\boldsymbol{K}_{12}$ becomes

$$\begin{aligned}\boldsymbol{K}_{12} &= \boldsymbol{j}\boldsymbol{K}_d\boldsymbol{j}^T \\ &= \begin{bmatrix} \mathrm{k}(2 + C_{2\theta}) & 0 & \mathrm{k}(d_2 - (d_1 + d_3)C_\theta) \\ & 2\mathrm{k}S_\theta^2 & (-d_1 + d_3)\,\mathrm{k}S_\theta \\ \textit{symm.} & & \mathrm{k}\left(d_1^2 + d_2^2 + d_3^2\right) \end{bmatrix},\end{aligned} \tag{45}$$

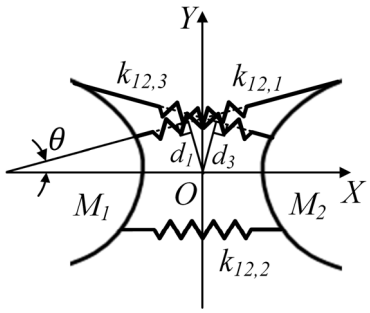

FIGURE 9. Geometric configuration of spring connections of K_{12} with full rank ($d_1 = d_3$, $\theta \neq 0$).

where $\boldsymbol{K}_d$ is the diagonal matrix of the spring constants, and $\boldsymbol{j}$ is the Jacobian matrix whose columns are the line vectors of the connected springs [11]. If all the spring constants of $\boldsymbol{K}_{12}$ are equal, the diagonal matrix can be expressed by $\boldsymbol{K}_d = diag(\mathrm{k}, \mathrm{k}, \mathrm{k})$. Moreover, Jacobian matrix $\boldsymbol{j}$ becomes $\begin{bmatrix} C_\theta & 1 & C_\theta \\ S_\theta & 0 & -S_\theta \\ -d_1 & d_2 & -d_3 \end{bmatrix}$, where d_P is the distance between the origin and the line of the Pth spring. Because d_1 equals d_3 in Fig. 9, $\boldsymbol{K}_{12}$ of (45) should satisfy the following relations for all configurations:

$$\begin{aligned} &\boldsymbol{K}_{12}\,(1,2)\,(=\boldsymbol{K}_{12}(2,1)) = 0 \quad \text{and} \\ &\boldsymbol{K}_{12}\,(2,3)\,(=\boldsymbol{K}_{12}(3,2)) = 0, \end{aligned} \tag{46}$$

where $\boldsymbol{K}_{12}\,(u, v)$ means the uth row and vth column of $\boldsymbol{K}_{12}$.

III. DESIGN METHOD

For the design of a symmetric dual-body system with prespecified ratios at six target resonant frequencies, the desired stiffness matrix can be determined from (14), (18-1) and (18-2)

$$\boldsymbol{K} = \boldsymbol{M}\boldsymbol{S}\left[\Omega^2\right]\boldsymbol{S}^{-1}, \tag{47}$$

where $\left[\Omega^2\right] = diag(\Omega_1^2, \Omega_2^2, \Omega_3^2, \Omega_4^2, \Omega_5^2, \Omega_6^2)$ and Ω_j is the jth target frequency. The stiffness matrix ($\boldsymbol{K}$) and modal matrix ($\boldsymbol{S}$) in (47) must satisfy the following five constraints for the realization of stiffness:

1) The first constraint is such that the orthogonality of the vibration modes (or, vibration centers) with respect to the inertia matrix has to be satisfied. We obtained (20) from this constraint and the coordinates of vibration centers given by (20) are rewritten in terms of c, α_P, and β_P (Fig. 10):

$$\begin{aligned} &x_{1,1} = c + \alpha_1, y_{1,1} = G/\alpha_2, \quad x_{1,3} = c - \alpha_3, \\ &x_{1,4} = c + \beta_1, y_{1,4} = \beta_2 \quad \text{and } x_{1,6} = c - \beta_3. \end{aligned} \tag{48}$$

To satisfy (20), the remaining coordinates of vibration centers can be written as

$$\begin{aligned} x_{1,2} &= \frac{G^2\,(G + c\alpha_3) + \alpha_2^2(G - c\alpha_1)(G - \alpha_1\alpha_3)}{G^2\alpha_3 + \alpha_2^2\alpha_1(-G + \alpha_1\alpha_3)}, \\ y_{1,2} &= \frac{\alpha_2 G^2(\alpha_1 + \alpha_3)}{-G^2\alpha_3 + \alpha_2^2\alpha_1(G - \alpha_1\alpha_3)}, \\ y_{1,3} &= \alpha_2\left(-1 + \frac{\alpha_1\alpha_3}{G}\right), \\ x_{1,5} &= \frac{G^2 + c\left(\beta_1^2 + \beta_2^2\right)\beta_3 + G(\beta_2^2 - \beta_1\,(c + \beta_3))}{-G\beta_1 + \left(\beta_1^2 + \beta_2^2\right)\beta_3}, \\ y_{1,5} &= \frac{G\beta_2(\beta_1 + \beta_3)}{G\beta_1 - \left(\beta_1^2 + \beta_2^2\right)\beta_3} \quad \text{and } y_{1,6} = \frac{-G + \beta_1\beta_3}{\beta_2}. \end{aligned} \tag{49}$$

2) Under the assumption of low damping with the identical modal damping ratio, i.e., $\zeta_j(j = 1, \cdots, 6) = \zeta$, another constraint was given by (42-1) and (42-2). If we substitute the coordinates obtained from the first constraint of (48) and (49) into (42-1) and (42-2), we obtain the expressions for the distances of α_1, α_3, β_1 and β_3 (Fig. 10) (Eqn. (50), as shown at the bottom of the page).

3) The geometrics symmetry conditions given by (46) are rewritten as $\boldsymbol{K}\,(1,5) = \boldsymbol{K}\,(2,6) = 0$. From (23), (47) and

$$\begin{aligned} \alpha_1 &= \pm\sqrt{\frac{G(-\alpha_2^2\Omega_1^2 + G\gamma_1\Omega_2^2 + G\gamma_2\Omega_3^2)}{\alpha_2^2\Omega_1^2}}, \\ \alpha_3 &= \frac{G\alpha_2^2\alpha_1\left(\Omega_1^2 + \gamma_1\Omega_2^2\right)}{G^2\gamma_1\Omega_2^2 + \alpha_2^2\left(-G\Omega_1^2 + \gamma_1\alpha_1^2\Omega_2^2\right)} \\ &\quad \pm\frac{\sqrt{G\gamma_1(G^2 + \alpha_2^2(G + \alpha_1^2))\Omega_2^2(\alpha_2^2(G + \alpha_1^2)\Omega_1^2 - G^2\gamma_1\Omega_2^2)}}{G^2\gamma_1\Omega_2^2 + \alpha_2^2(-G\Omega_1^2 + \gamma_1\alpha_1^2\Omega_2^2)}, \\ \beta_1 &= \pm\sqrt{\frac{(G + \beta_2^2)\Omega_4^2}{\gamma_4'\Omega_5^2 + \gamma_5'\Omega_6^2}} \quad \text{and} \\ \beta_3 &= \frac{-G\beta_1\left(G + \beta_2^2\right)\Omega_4^2 \pm G\gamma_4'\beta_1^3\Omega_5^2}{\beta_1^2\left(-G\Omega_4^2 + \gamma_4'\left(\beta_1^2 + \beta_2^2\right)\Omega_5^2\right)} \\ &\quad + \frac{\sqrt{G\gamma_4'\beta_1^2\beta_2^2(G + \beta_1^2 + \beta_2^2)\Omega_5^2((G + \beta_2^2)\Omega_4^2 - \gamma_4'\beta_1^2\Omega_5^2)}}{\beta_1^2(-G\Omega_4^2 + \gamma_4'(\beta_1^2 + \beta_2^2)\Omega_5^2)}. \end{aligned} \tag{50}$$

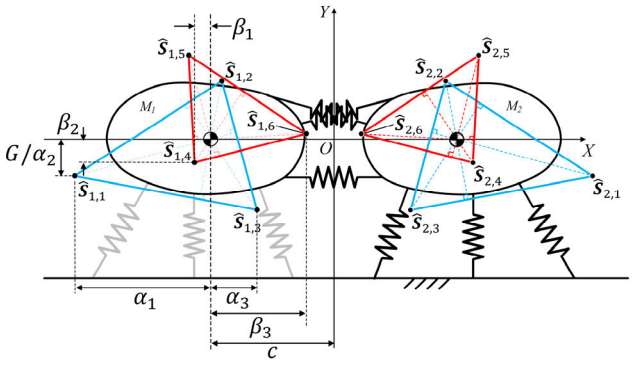

FIGURE 10. Design variables.

(A1), $\boldsymbol{K}(1,5)$ and $\boldsymbol{K}(2,6)$ can be determined by

$$\boldsymbol{K}(1,5) = \frac{1}{2}m(a_1+a_2) = 0 \quad \text{and}$$
$$\boldsymbol{K}(2,6) = \frac{1}{2}m(b_1+b_2+c(b_3+b_4)) = 0, \qquad (51)$$

where the detailed expressions of a_1, a_2 and $b_1, \cdots, b_4$ in (51) are given in Appendix B. Since m of (51) is not zero, (51) becomes

$$a_1 + a_2 = 0 \quad \text{and} \quad b_1 + b_2 + c(b_3 + b_4) = 0. \qquad (52)$$

If we choose β_2 as a free variable, α_2 and c can be determined from the substitution of (48), (49) and (50) into (52). The expressions of α_2 and c can be obtained by use of any symbolic computation software such as Mathematica. However, to avoid complexity of presentation, α_2 and c may be expressed briefly as (Fig. 10)

$$\alpha_2 = f(a_2, G, \gamma_1, \gamma_2, \Omega_P) \quad \text{and}$$
$$c = f(G, \alpha_P, \beta_P, \Omega_j). \qquad (53)$$

4) The angle of the base excitation force ψ_B is determined by (44).

5) Since the spring constants are positive, $\boldsymbol{K}_1$, $\boldsymbol{K}_2$ and $\boldsymbol{K}_{12}$ must be positive definite. Therefore, positive definiteness of $\boldsymbol{K}_1$, $\boldsymbol{K}_2$ and $\boldsymbol{K}_{12}$ has to be checked.

The design process is summarized in a flow chart as shown in Fig. 11.

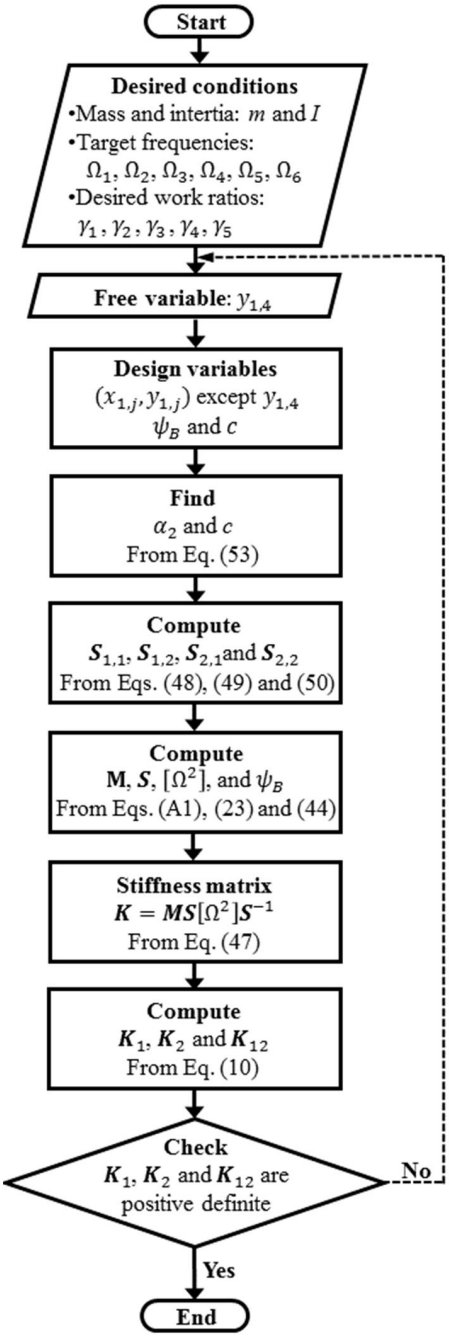

FIGURE 11. Flow chart for deriving the stiffness matrices $\boldsymbol{K}_1$, $\boldsymbol{K}_2$, and $\boldsymbol{K}_{12}$ of symmetric dual-body system with prespecified work ratios at six target frequencies.

IV. NUMERICAL EXAMPLES

In order to demonstrate the usefulness of the proposed design method, one design example of a vibration energy harvester is presented. It will be shown how to improve the performance of harvester significantly while widening the valid working bandwidth within a target range of frequency.

In this section, four symmetric dual-body systems (energy harvesters) subject to base excitation are designed to illustrate the design process and advantages of the proposed method. All of four systems are assumed to have identical mass and moment of inertia of $m = 4.3$ kg and $I = 0.17$ kgm^2, respectively. In addition, f_B of 15 N and β_2 of -0.8 m are selected. The range of the desired bandwidth is determined to be from 100 Hz to 125 Hz and the six target resonant frequencies are specified as:

$$\Omega_1 = 100 \text{ Hz}, \Omega_2 = 110 \text{ Hz}, \Omega_3 = 125 \text{ Hz},$$
$$\Omega_4 = 120 \text{ Hz}, \Omega_5 = 115 \text{ Hz and } \Omega_6 = 105 \text{ Hz}. \qquad (54)$$

The work ratios in each system are set as follows:

System 1 : $1 : \gamma_1 : \gamma_2 : \gamma_3 : \gamma_4 : \gamma_5 = 1 : 1 : 1 : 1 : 1 : 1$,

System 2 : $1 : \gamma_1 : \gamma_2 : \gamma_3 : \gamma_4 : \gamma_5$
$= 1 : 0.5 : 0.25 : 1 : 1 : 1$,

$$\begin{aligned}\textbf{System 3}&: 1:\gamma_1:\gamma_2:\gamma_3:\gamma_4:\gamma_5\\ &= 1:1:1:1:2:3 \quad \text{and}\\ \textbf{System 4}&: 1:\gamma_1:\gamma_2:\gamma_3:\gamma_4:\gamma_5\\ &= 1:0.7:0.25:0.4:0.55:0.85. \end{aligned} \tag{55}$$

The frequency response plots of all the above systems will be shown (Fig. 13), detailed explanation of the design process will be given only for the case of **System 1**. Referring to the design process (Fig. 11), the first step of the design is to find α_2 and c from (53) and

$$\alpha_2 = 0.3278 \text{ m} \quad \text{and } c = 1.1918 \text{ m}. \tag{56}$$

Using (48), (49) and (50), the $\boldsymbol{S}_{n,1}$ and $\boldsymbol{S}_{n,2}$ are computed as

$$\begin{aligned}\boldsymbol{S}_{1,1} &= \begin{bmatrix} 0.1206 & -0.4873 & -0.2690\\ -1.1636 & -0.5111 & -1.4425\\ 1.0000 & 1.0000 & 1.0000 \end{bmatrix},\\ \boldsymbol{S}_{1,2} &= \begin{bmatrix} -0.8000 & -0.0716 & 0.1860\\ -1.8270 & -1.0394 & -1.3638\\ 1.0000 & 1.0000 & 1.0000 \end{bmatrix},\\ \boldsymbol{S}_{2,1} &= \begin{bmatrix} 0.1206 & -0.4873 & -0.2690\\ 1.1636 & 0.5111 & 1.4425\\ 1.0000 & 1.0000 & 1.0000 \end{bmatrix} \quad \text{and}\\ -\boldsymbol{S}_{2,2} &= -\begin{bmatrix} -0.8000 & -0.0716 & 0.1860\\ 1.8270 & 1.0394 & 1.3638\\ 1.0000 & 1.0000 & 1.0000 \end{bmatrix}, \end{aligned} \tag{57}$$

where α_1, α_3, β_1 and β_3, as shown at the bottom of the page. The modal triangles formed by the normal modes of $\boldsymbol{S}_{1,1}$, $\boldsymbol{S}_{1,2}$, $\boldsymbol{S}_{2,1}$, and $\boldsymbol{S}_{2,2}$ are shown in Fig. 12(a).

The next step is determining the inertia and modal matrices of the system from (A1) and (23):

$$\boldsymbol{M} = \begin{bmatrix} 4.3000 & 0.0000 & 0.0000\\ 0.0000 & 4.3000 & 5.1248\\ 0.0000 & 5.1248 & 6.2779 \end{bmatrix} \quad \boldsymbol{0} \in R^{3\times 3}$$

$$\boldsymbol{0} \in R^{3\times 3} \quad \begin{bmatrix} 4.3000 & 0.0000 & 0.0000\\ 0.0000 & 4.3000 & -5.1248\\ 0.0000 & -5.1248 & 6.2779 \end{bmatrix} \quad \text{and}$$

$$\boldsymbol{S} = \begin{bmatrix} 0.1206 & -0.4873 & -0.2690\\ -1.1636 & -0.5111 & -1.4425\\ 1.0000 & 1.0000 & 1.0000\\ 0.1206 & -0.4873 & -0.2690\\ 1.1636 & 0.5111 & 1.4425\\ 1.0000 & 1.0000 & 1.0000 \end{bmatrix} \begin{bmatrix} -0.8000 & -0.0716 & 0.1860\\ -1.8270 & -1.0394 & -1.3638\\ 1.0000 & 1.0000 & 1.0000\\ 0.8000 & 0.0716 & -0.1860\\ -1.8270 & -1.0394 & -1.3638\\ -1.0000 & -1.0000 & -1.0000 \end{bmatrix}. \tag{58}$$

Now, the angle of the base excitation force ψ_B of 45.3470° can be found from (44). Finally, the stiffness matrix is determined by (47)

$$\boldsymbol{K} = 10^6 \begin{bmatrix} 2.2229 & 0.2088 & 0.1990\\ & 2.2384 & 2.6571\\ \textit{symm.} & & 3.2340 \end{bmatrix} \quad \textit{symm.}$$

$$\begin{aligned}\alpha_1 &= -\sqrt{\frac{G(-\alpha_2^2\Omega_1^2 + G\gamma_1\Omega_2^2 + G\gamma_2\Omega_3^2)}{\alpha_2^2\Omega_1^2}},\\ \alpha_3 &= \frac{G\alpha_2^2\alpha_1\left(\Omega_1^2+\gamma_1\Omega_2^2\right)}{G^2\gamma_1\Omega_2^2+\alpha_2^2\left(-G\Omega_1^2+\gamma_1\alpha_1^2\Omega_2^2\right)}\\ &\quad + \frac{\sqrt{G\gamma_1(G^2+\alpha_2^2(G+\alpha_1^2))\Omega_2^2(\alpha_2^2(G+\alpha_1^2)\Omega_1^2 - G^2\gamma_1\Omega_2^2)}}{G^2\gamma_1\Omega_2^2+\alpha_2^2(-G\Omega_1^2+\gamma_1\alpha_1^2\Omega_2^2)},\\ \beta_1 &= \sqrt{\frac{(G+\beta_2^2)\Omega_4^2}{\gamma_4'\Omega_5^2+\gamma_5'\Omega_6^2}} \quad \text{and}\\ \beta_3 &= \frac{-G\beta_1\left(G+\beta_2^2\right)\Omega_4^2 + G\gamma_4'\beta_1^3\Omega_5^2}{\beta_1^2\left(-G\Omega_4^2+\gamma_4'\left(\beta_1^2+\beta_2^2\right)\Omega_5^2\right)}\\ &\quad + \frac{\sqrt{G\gamma_4'\beta_1^2\beta_2^2(G+\beta_1^2+\beta_2^2)\Omega_5^2((G+\beta_2^2)\Omega_4^2 - \gamma_4'\beta_1^2\Omega_5^2)}}{\beta_1^2(-G\Omega_4^2+\gamma_4'(\beta_1^2+\beta_2^2)\Omega_5^2)}. \end{aligned}$$

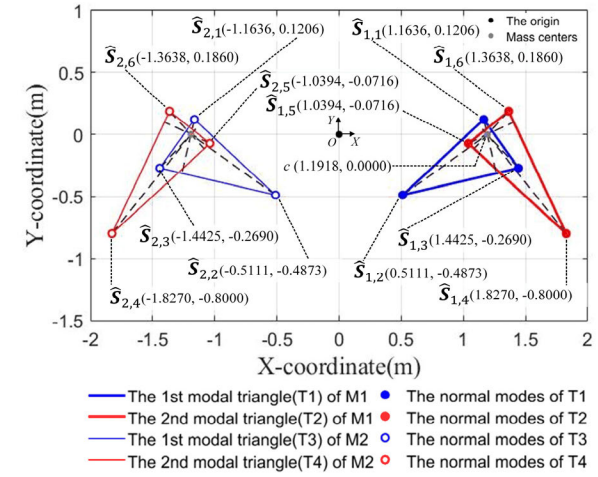

(a)

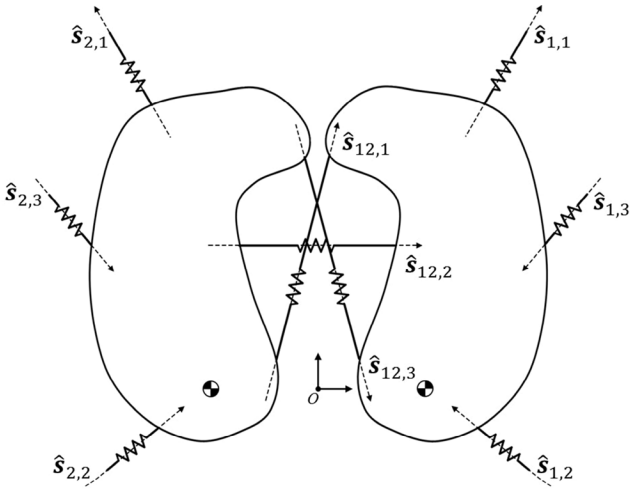

(b)

FIGURE 12. (a) Vibration centers of normal modes, modal triangles, and (b) one feasible realization of the designed stiffness matrix with the work ratio of 1:1:1:1:1:1.

$$\begin{bmatrix} -0.0155 & 0.0000 & -0.0175 \\ & -0.0256 & 0.0000 \\ symm. & & -0.0399 \\ 2.2229 & -0.2088 & 0.1990 \\ & 2.2384 & -2.6571 \\ symm. & & 3.2340 \end{bmatrix}. \quad (59)$$

Thus, the stiffness matrices ($\boldsymbol{K}_1$, $\boldsymbol{K}_2$, and $\boldsymbol{K}_{12}$) are determined as

$$\boldsymbol{K}_1 = 10^6 \begin{bmatrix} 2.2074 & 0.2088 & 0.1814 \\ & 2.2128 & 2.6571 \\ symm. & & 3.1942 \end{bmatrix},$$

$$\boldsymbol{K}_{12} = 10^5 \begin{bmatrix} 0.1546 & 0.0000 & 0.1755 \\ & 0.2561 & 0.0000 \\ symm. & & 0.3989 \end{bmatrix} \quad \text{and}$$

$$\boldsymbol{K}_2 = 10^6 \begin{bmatrix} 2.2074 & -0.2088 & 0.1814 \\ & 2.2128 & -2.6571 \\ symm. & & 3.1942 \end{bmatrix}. \quad (60)$$

TABLE 1. Line vectors and spring constants for feasible realization.

P	1	2	3
$k_{1,P}$	0.0013	2.0035	2.4154
$\hat{\boldsymbol{s}}_{1,P}$	$\begin{bmatrix}0.5000\\0.8660\\0.0510\end{bmatrix}$	$\begin{bmatrix}-0.7660\\0.6428\\0.7982\end{bmatrix}$	$\begin{bmatrix}-0.6535\\-0.7570\\-0.8911\end{bmatrix}$
$k_{12,P}$	0.0137	0.0137	0.0137
$\hat{\boldsymbol{s}}_{12,P}$	$\begin{bmatrix}0.2543\\0.9671\\-0.5152\end{bmatrix}$	$\begin{bmatrix}1.0000\\0.0000\\1.5434\end{bmatrix}$	$\begin{bmatrix}0.2543\\-0.9671\\0.5152\end{bmatrix}$
$k_{2,P}$	0.0013	2.0035	2.4154
$\hat{\boldsymbol{s}}_{2,P}$	$\begin{bmatrix}-0.5000\\0.8660\\-0.0510\end{bmatrix}$	$\begin{bmatrix}0.7660\\0.6428\\-0.7982\end{bmatrix}$	$\begin{bmatrix}0.6535\\-0.7570\\0.8911\end{bmatrix}$

k: $\times 10^6\ Nm^{-1}$

$\boldsymbol{K}_1$, $\boldsymbol{K}_2$, and $\boldsymbol{K}_{12}$ can be realized by means of parallel connection of line springs using the technique presented in [13]. The line vectors and the spring constants are determined and listed in Table 1. Fig. 12(b) shows one feasible realization of stiffness by means of nine linear springs.

The work produced by the base excitation are computed. The frequency responses for four different work ratios and damping ratios are shown in Fig. 13. Table 2 shows the simulated values of peaks and their work ratios for the different damping ratios of **System 1**.

V. COMPARISON AND DISCUSSION OF RESULTS

The meanings of the working bandwidth can be used differently according to the researches, e.g., the frequency band is defined where the output voltage is -3 dB of the peak value in [14]. In this study, the working bandwidth means the frequency range within which the energy magnitude remains over the minimum value to operate electronic circuits. The energy magnitude can be set depending on the desired electronic circuits and sensors. In vibration harvesters, the performances of systems can be improved when the working bandwidth is widened. However, the energy peaks of typical vibration harvesters rise and drop steeply in narrow range nearby resonant frequencies, and it overshadows the meaning of the working bandwidth which maintains the power over the desired level.

Fig. 14 shows the frequency responses of three different vibration systems in the target frequency range, which is determined from 10 Hz to 60 Hz because the frequencies of ambient vibration sources are variable in the low frequency range within 100 Hz [15], [16]. The dotted curve is the simulated result using the design method by Kim, and the detailed description of the design method can be found in [1]. It depicts the frequency response of a single-body system, which is designed for the work ratio of 1:1:1 at three target frequencies (35 Hz, 45 Hz and 55 Hz). To compare the single-body system with the dual-body system, the dotted curve is plotted using double values of the frequency response of the single-body system. The dashed curve shows the frequency response of the dual-body system considering only the six target frequencies, i.e., 30 Hz, 35 Hz, 40 Hz, 45 Hz, 50 Hz,

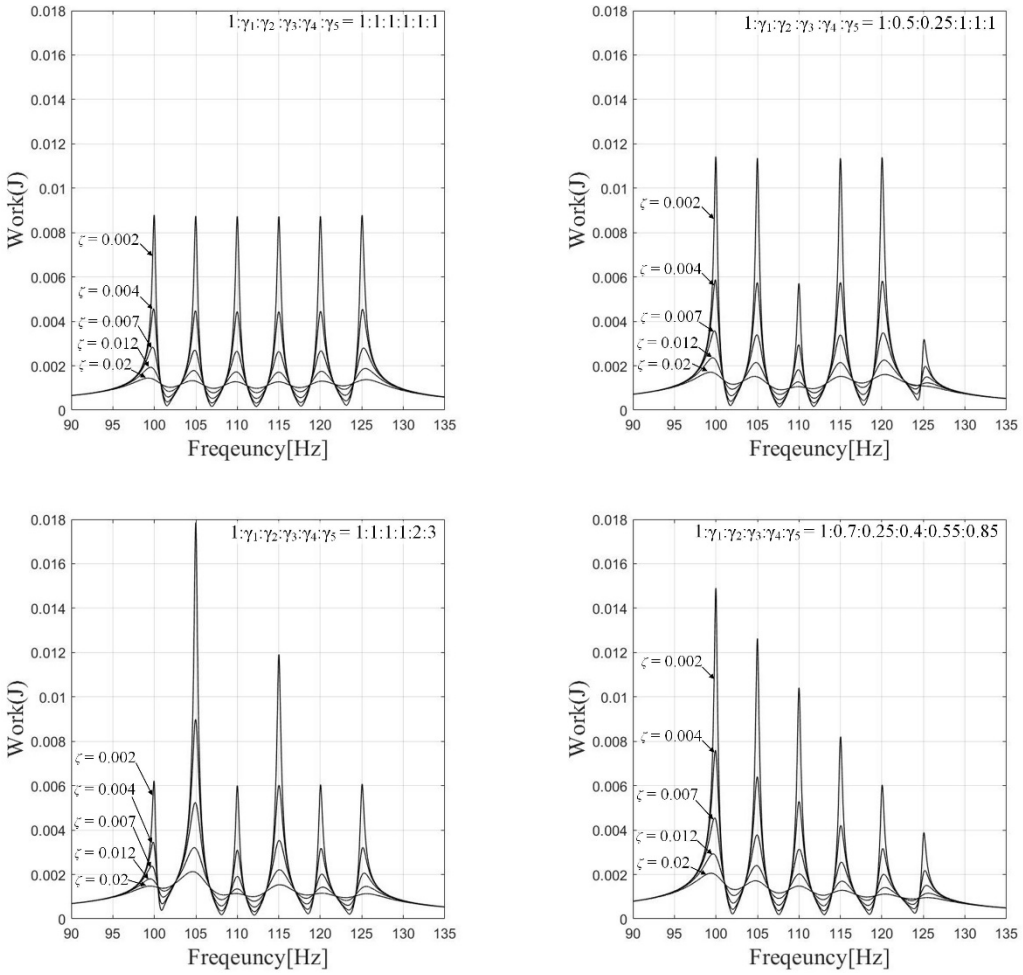

FIGURE 13. Frequency responses for four different work ratios and diverse damping ratios at target resonant frequencies of (54).

TABLE 2. Simulated values of peaks and work ratios for different damping ratios of System 1.

ζ	Simulated values of energy (J)						Ratios of W_j
	W_1	W_2	W_3	W_4	W_5	W_6	
0.002	0.00875	0.00873	0.00872	0.00872	0.00873	0.00875	1.000:0.9980:0.9974:0.9973:0.9980:1.0002
0.004	0.00448	0.00445	0.00443	0.00443	0.00444	0.00448	1.000:0.9926:0.9900:0.9899:0.9925:1.0005
0.007	0.00271	0.00266	0.00264	0.00264	0.00266	0.00272	1.000:0.9805:0.9737:0.9735:0.9803:1.0008
0.012	0.00181	0.00174	0.00172	0.00172	0.00174	0.00181	1.000:0.9607:0.9463:0.9461:0.9606:0.9984
0.02	0.00137	0.00130	0.00127	0.00127	0.00130	0.00135	1.000:0.9491:0.9285:0.9287:0.9488:0.9851

and 55 Hz, without using any specified work ratio. The solid curve represents the frequency response of the dual-body system with the work ratio of 1:1:1:1:1:1 at the same six target frequencies.

Referring to Fig. 14, it is noted that the heights of the valleys of the dual-body system designed for the specified work ratio are raised significantly comparing to the other two systems. This could be an important research issue in designing a vibration system such as a vibration energy harvester which requires a practically wide bandwidth. The energy peaks generated at resonant frequencies by a typical vibration energy harvester drop immediately and significantly when a slight deviation of the operating frequency from resonant frequencies occurs. However, Fig. 14 shows that the dual-body system designed for the specified work ratio has a practically wide working bandwidth. Moreover, the dashed and solid curves show that the work ratio is an important component to widen the working bandwidth.

The working bandwidths of some previous researches are summarized in Table 3. To compare the results, the working bandwidth is calculated by the sum of the frequency ranges over 60 % of the maximum peak value in the target frequency

TABLE 3. Working bandwidths of published energy harvesters and this research.

Reference	Type	The number of resonant frequencies in target frequency range (10 Hz – 60 Hz)	Frequency ranges over 60 % of the maximum peak value in target frequency range (Hz)	working bandwidth [=EB]	Rate*
Qi et al. (2010) [17]	C	-	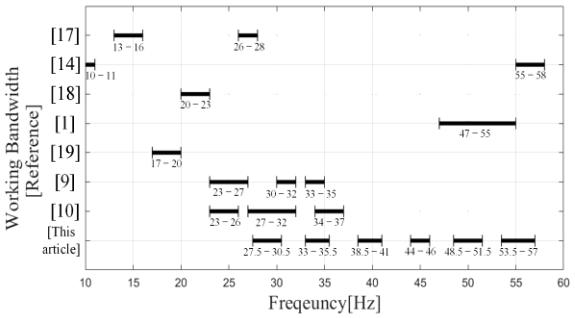	5 Hz	10 %
Seo et al. (2012) [14]	C	3		4 Hz	8 %
Bai et al. (2014) [18]	C	5		3 Hz	6 %
Kim et al. (2015) [1]	-	3		8 Hz	16 %
Park et al. (2017) [19]	-	3		3 Hz	6 %
Kim et al. (2017) [9]	S	3		8 Hz	16 %
Kim et al. (2019) [10]	S	3		11 Hz	22 %
This article	-	6		16.5 Hz	33 %

C: Cantilever beam type, S: Serial linkage type, and *rate of the working bandwidth in target frequency range, which is calculated by $\frac{\text{EB(Hz)}}{\text{50(Hz)}} \times 100$.

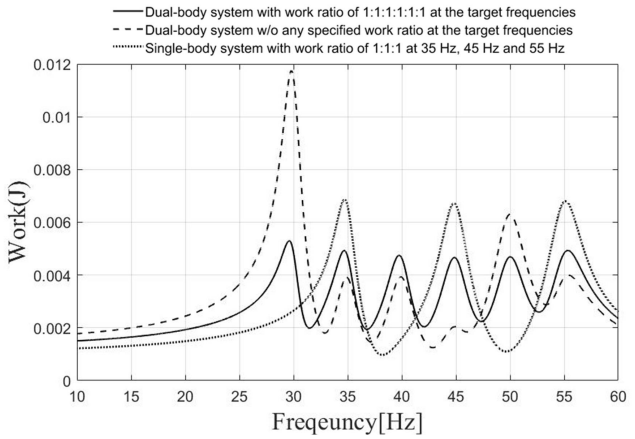

FIGURE 14. Frequency responses of three different systems.

range (10 Hz – 60 Hz). The working bandwidths of the systems by Bai and Park are narrow although they have five and three resonant frequencies. It is because the differences of peak values are large. By locating the six target resonant frequencies in the target frequency range and adjusting work ratio to 1:1:1:1:1:1 in this research, the rate of the working bandwidth in the target frequency range could be widened to 33 %.

VI. CONCLUSION

A novel design method to develop a vibration system with desired work ratios at six target resonant frequencies is introduced. The number of peaks, which is a significant design factor for a broad bandwidth, increases to six by using a planar symmetric dual-body system. An important contribution of this work lies in introducing geometrical representation of vibration modes of a symmetric dual-body system together with its applications. One rigid-body of a dual-body system has six vibration modes and they are divided into two groups of three vibration modes. Each group of three vibration modes forms a modal triangle whose orthocenter coincides with the mass center. By obtaining the geometric relations of two modal triangles from the orthogonality of vibration modes, the design method has been developed to realize the symmetric dual-body system that satisfies the requirements for six resonant frequencies as well as the work ratios.

APPENDIX A

The derivation of the relation between the time-independent displacements of two rigid bodies in a planar symmetric dual-body vibration system (i.e., $\hat{\boldsymbol{D}}_1$ and $\hat{\boldsymbol{D}}_2$) is described in Appendix A. Above all, the inertia matrices ($\boldsymbol{M}_1$ and $\boldsymbol{M}_2$) of (10) can be expressed by

$$\begin{aligned}\boldsymbol{M}_1 &= \boldsymbol{E}_1^T \begin{bmatrix} m & & \\ & m & \\ & & I \end{bmatrix} \boldsymbol{E}_1 \\ &= \begin{bmatrix} m & 0 & 0 \\ 0 & m & cm \\ 0 & cm & I + c^2 m \end{bmatrix} \quad \text{and} \\ \boldsymbol{M}_2 &= \boldsymbol{E}_2^T \begin{bmatrix} m & & \\ & m & \\ & & I \end{bmatrix} \boldsymbol{E}_2 \\ &= \begin{bmatrix} m & 0 & 0 \\ 0 & m & -cm \\ 0 & -cm & I + c^2 m \end{bmatrix}, \end{aligned} \tag{A.1}$$

where $\boldsymbol{E}_1 \left(= \begin{bmatrix} 1 & 0 & 0 \\ 0 & 1 & c \\ 0 & 0 & 1 \end{bmatrix}\right)$ and $\boldsymbol{E}_2 \left(= \begin{bmatrix} 1 & 0 & 0 \\ 0 & 1 & -c \\ 0 & 0 & 1 \end{bmatrix}\right)$ are transformation matrices. c is the distance between the the mass center of each rigid body and the origin. Furthermore, the configurations of springs composing $\boldsymbol{K}_1$, $\boldsymbol{K}_2$ and $\boldsymbol{K}_{12}$ are symmetrical about the Y-axis, using representative symbols

$(k_{1,PQ})$ and $(k_{12,PQ})$, they can be expressed by

$$\boldsymbol{K}_1 = \begin{bmatrix} k_{1,11} & k_{1,12} & k_{1,13} \\ & k_{1,22} & k_{1,23} \\ symm. & & k_{1,33} \end{bmatrix},$$
$$\boldsymbol{K}_2 = \begin{bmatrix} k_{1,11} & -k_{1,12} & k_{1,13} \\ & k_{1,22} & -k_{1,23} \\ symm. & & k_{1,33} \end{bmatrix} \quad \text{and}$$
$$\boldsymbol{K}_{12} = \begin{bmatrix} k_{12,11} & 0 & k_{12,13} \\ & k_{12,22} & 0 \\ symm. & & k_{12,33} \end{bmatrix}, \tag{A.2}$$

where $k_{1(or\ 12),PQ}$ is the component of the Pth row and Qth column in $\boldsymbol{K}_1$(or $\boldsymbol{K}_{12}$). Substituting (A1), (A2) and (12) into (14) yields

$$\begin{bmatrix} \Xi_1 & \Xi_2 & \Xi_3 & \Xi_4 & \Xi_5 & \Xi_6 \end{bmatrix}^T = \begin{bmatrix} 0 & 0 & 0 & 0 & 0 & 0 \end{bmatrix}^T, \tag{A.3}$$

where

$$\begin{aligned}
\Xi_1 &= -\delta x_2 k_{12,11} + \delta y_1 k_{1,12} - \delta\varphi_2 k_{12,13} \\
&\quad + \delta\varphi_1 \left(k_{1,13} + k_{12,13}\right) + \delta x_1 (k_{1,11} + k_{12,11} - \omega^2 m), \\
\Xi_2 &= \delta x_1 k_{1,12} - \delta y_2 k_{12,22} + \delta\varphi_1 k_{1,23} \\
&\quad + \delta y_1 \left(k_{1,22} + k_{12,22} - \omega^2 m\right), \\
\Xi_3 &= -\delta x_2 k_{12,13} + \delta x_1 \left(k_{1,13} + k_{12,13}\right) + \delta y_1 k_{1,23} \\
&\quad - \delta\varphi_2 k_{12,33} + \delta\varphi_1 (k_{1,33} + k_{12,33} - \omega^2 (I + mc^2)), \\
\Xi_4 &= -\delta\varphi_1 k_{12,11} - \delta y_2 k_{1,12} - \delta\varphi_1 k_{12,13} \\
&\quad + \delta\varphi_2 \left(k_{1,13} + k_{12,13}\right) + \delta x_2 (k_{1,11} + k_{12,11} - \omega^2 m), \\
\Xi_5 &= -\delta x_2 k_{1,12} - \delta y_1 k_{12,22} - \delta\varphi_2 k_{1,23} \\
&\quad + \delta y_2 (k_{1,22} + k_{12,22} - \omega^2 m) \quad \text{and} \\
\Xi_6 &= -\delta x_1 k_{12,13} + \delta x_2 \left(k_{1,13} + k_{12,13}\right) - \delta y_2 k_{1,23} \\
&\quad - \delta\varphi_1 k_{12,33} + \delta\varphi_2 (k_{1,33} + k_{12,33} - \omega^2 (I + mc^2)).
\end{aligned}$$

By canceling ω in (A3), (A3) can be simplified, and it is performed using two approaches: 1) $\Xi_1 + \Xi_4$, $\Xi_2 - \Xi_5$, $\Xi_3 + \Xi_6$ and 2) $\Xi_1 - \Xi_4$, $\Xi_2 + \Xi_5$, $\Xi_3 - \Xi_6$. From approach 1), (A3) is simplified to

$$\begin{bmatrix} \Gamma_1 & 0 & 0 \\ 0 & \Gamma_2 & 0 \\ 0 & 0 & \Gamma_3 \end{bmatrix} \begin{bmatrix} \delta\varphi_1 + \delta\varphi_2 \\ \delta y_1 - \delta y_2 \\ \delta x_1 + \delta x_2 \end{bmatrix} = \mathbf{0}, \tag{A.4}$$

where Γ_1, Γ_2, and Γ_3, as shown at the bottom of the page. If Γ_1, Γ_2, and Γ_3 cannot be zeros, the remaining terms of each equation of (A4) should be zeros. Thus, the relations between time-independent displacements are derived as

$$\delta x_1 = -\delta x_2,\ \delta y_1 = \delta y_2 \quad \text{and} \quad \delta\varphi_1 = -\delta\varphi_2. \tag{A.5}$$

Similarly, approach 2) yields

$$(\delta\varphi_1 - \delta\varphi_2)\,\Gamma_4 = 0,\ \ (\delta y_1 + \delta y_2)\,\Gamma_5 = 0 \quad \text{and} \quad (\delta x_1 - \delta x_2)\,\Gamma_6 = 0, \tag{A.6}$$

where Γ_4, Γ_5, and Γ_6, as shown at the bottom of the page. Accordingly, the other relations between the time-independent displacements are derived:

$$\delta x_1 = \delta x_2,\ \ \delta y_1 = -\delta y_2 \quad \text{and} \quad \delta\varphi_1 = \delta\varphi_2. \tag{A.7}$$

$$\Gamma_1 = \begin{pmatrix} k_{1,33} - \dfrac{k_{1,23}\left(k_{1,12}k_{1,13} - k_{1,11}k_{1,23} + k_{1,23}\omega^2 m\right)}{k_{1,12}^2 + \left(k_{1,11} - \omega^2 m\right)\left(-k_{1,22} - 2k_{12,22} + \omega^2 m\right)} \\ + \dfrac{k_{1,13}\left(-k_{1,12}k_{1,23} + k_{1,13}\left(k_{1,22} + 2k_{12,22} - \omega^2 m\right)\right)}{k_{1,12}^2 + \left(k_{1,11} - \omega^2 m\right)\left(-k_{1,22} - 2k_{12,22} + \omega^2 m\right)} \\ -\omega^2\left(I + mc^2\right) \end{pmatrix},$$
$$\Gamma_2 = \left(k_{1,22} + 2k_{12,22} - \omega^2 m + \frac{k_{1,12}^2}{-k_{1,11} + \omega^2 m}\right) \quad \text{and}$$
$$\Gamma_3 = \left(k_{1,11} - \omega^2 m\right).$$

$$\Gamma_4 = \begin{pmatrix} k_{1,33} + 2k_{12,33} \\ + \dfrac{k_{1,23}\left(-k_{1,12}\left(k_{1,13} + 2k_{12,13}\right) + k_{1,23}\left(k_{1,11} + 2k_{12,11} - \omega^2 m\right)\right)}{k_{1,12}^2 + \left(k_{1,11} + 2k_{12,11} - \omega^2 m\right)\left(-k_{1,22} + \omega^2 m\right)} \\ + \dfrac{\left(k_{1,13} + 2k_{12,13}\right)\left(-k_{1,12}k_{1,23} + \left(k_{1,13} + 2k_{12,13}\right)\left(k_{1,22} - \omega^2 m\right)\right)}{k_{1,12}^2 + \left(k_{1,11} + 2k_{12,11} - \omega^2 m\right)\left(-k_{1,22} + \omega^2 m\right)} \\ -\omega^2(I + mc^2) \end{pmatrix},$$
$$\Gamma_5 = \left(k_{1,22} - \omega^2 m - \frac{k_{1,12}^2}{k_{1,11} + 2k_{12,11} - \omega^2 m}\right) \quad \text{and}$$
$$\Gamma_6 = \left(k_{1,11} + 2k_{12,11} - \omega^2 m\right).$$

$$
\begin{aligned}
a_1 &= \frac{\Omega_1^2 y_{1,1}\left(y_{1,2}-y_{1,3}\right)+\Omega_2^2 y_{1,2}(-y_{1,1}+y_{1,3})+\Omega_3^2 y_{1,3}\left(y_{1,1}-y_{1,2}\right)}{x_{1,1}(y_{1,2}-y_{1,3})+x_{1,2}(-y_{1,1}+y_{1,3})+x_{1,3}(y_{1,1}-y_{1,2})},\\
a_2 &= \frac{\Omega_4^2 y_{1,4}\left(-y_{1,5}+y_{1,6}\right)+\Omega_5^2 y_{1,5}(y_{1,4}-y_{1,6})+\Omega_6^2 y_{1,6}\left(-y_{1,4}+y_{1,5}\right)}{x_{1,4}\left(y_{1,5}-y_{1,6}\right)+x_{1,5}\left(-y_{1,4}+y_{1,6}\right)+x_{1,6}(y_{1,4}-y_{1,5})},\\
b_1 &= \frac{\left(-\Omega_2^2+\Omega_3^2\right)x_{1,2}x_{1,3}y_{1,1}+\left(\Omega_1^2-\Omega_3^2\right)x_{1,1}x_{1,3}y_{1,2}}{x_{1,1}\left(y_{1,2}-y_{1,3}\right)+x_{1,2}\left(-y_{1,1}+y_{1,3}\right)+x_{1,3}\left(y_{1,1}-y_{1,2}\right)}\\
&\quad+\frac{\left(-\Omega_1^2+\Omega_2^2\right)x_{1,1}x_{1,2}y_{1,3}}{x_{1,1}\left(y_{1,2}-y_{1,3}\right)+x_{1,2}\left(-y_{1,1}+y_{1,3}\right)+x_{1,3}(y_{1,1}-y_{1,2})},\\
b_2 &= \frac{\left(\Omega_5^2-\Omega_6^2\right)x_{1,5}x_{1,6}y_{1,4}+\left(-\Omega_4^2+\Omega_6^2\right)x_{1,4}x_{1,6}y_{1,5}}{x_{1,4}\left(y_{1,5}-y_{1,6}\right)+x_{1,5}\left(-y_{1,4}+y_{1,6}\right)+x_{1,6}\left(y_{1,4}-y_{1,5}\right)}\\
&\quad+\frac{\left(\Omega_4^2-\Omega_5^2\right)x_{1,4}x_{1,5}y_{1,6}}{x_{1,4}\left(y_{1,5}-y_{1,6}\right)+x_{1,5}\left(-y_{1,4}+y_{1,6}\right)+x_{1,6}(y_{1,4}-y_{1,5})},\\
b_3 &= \frac{\Omega_3^2 x_{1,2}y_{1,1}-\Omega_2^2 x_{1,3}y_{1,1}-\Omega_3^2 x_{1,1}y_{1,2}+\Omega_1^2 x_{1,3}y_{1,2}}{x_{1,1}(-y_{1,2}+y_{1,3})+x_{1,2}\left(y_{1,1}-y_{1,3}\right)x_{1,3}\left(-y_{1,1}+y_{1,2}\right)}\\
&\quad+\frac{\Omega_2^2 x_{1,1}y_{1,3}-\Omega_1^2 x_{1,2}y_{1,3}}{x_{1,1}(-y_{1,2}+y_{1,3})+x_{1,2}\left(y_{1,1}-y_{1,3}\right)x_{1,3}\left(-y_{1,1}+y_{1,2}\right)} \quad \text{and}\\
b_4 &= \frac{-\Omega_6^2 x_{1,5}y_{1,4}+\Omega_5^2 x_{1,6}y_{1,4}+\Omega_6^2 x_{1,4}y_{1,5}-\Omega_4^2 x_{1,6}y_{1,5}}{x_{1,4}\left(-y_{1,5}+y_{1,6}\right)+x_{1,5}\left(y_{1,4}-y_{1,6}\right)x_{1,6}\left(-y_{1,4}+y_{1,5}\right)}\\
&\quad+\frac{-\Omega_5^2 x_{1,4}y_{1,6}+\Omega_4^2 x_{1,5}y_{1,6}}{x_{1,4}\left(-y_{1,5}+y_{1,6}\right)+x_{1,5}\left(y_{1,4}-y_{1,6}\right)x_{1,6}\left(-y_{1,4}+y_{1,5}\right)}.
\end{aligned}
$$

In (A5) and (A7), the relation between the magnitudes of small angular displacements is expressed by

$$\|\delta\varphi_1\| = \|\delta\varphi_2\|. \tag{A.8}$$

Furthermore, the configuration of the normal mode which is normalized by $\delta\varphi_1$ is represented as two types

$$
\begin{aligned}
&\left[\frac{\delta x_1}{\delta\varphi_1}\quad\frac{\delta y_1}{\delta\varphi_1}\quad 1\quad -\frac{\delta x_1}{\delta\varphi_1}\quad\frac{\delta y_1}{\delta\varphi_1}\quad -1\right]^T \quad \text{and}\\
&\left[\frac{\delta x_1}{\delta\varphi_1}\quad\frac{\delta y_1}{\delta\varphi_1}\quad 1\quad \frac{\delta x_1}{\delta\varphi_1}\quad -\frac{\delta y_1}{\delta\varphi_1}\quad 1\right]^T.
\end{aligned} \tag{A.9}
$$

From (A8) and (A9), it can be checked that the normal modes of two rigid bodies are located symmetrically about the Y-axis and the magnitudes of small angular displacements are equal.

APPENDIX B

a_1, a_2, b_1, b_2, b_3, and b_4, as shown at the top of the page.

REFERENCES

[1] J. W. Kim, S. Lee, and Y. J. Choi, "Design method of planar vibration system for specified ratio of energy peaks," *J. Sound Vib.*, vol. 344, pp. 363–376, May 2015.

[2] S. M. Shahruz, "Design of mechanical band-pass filters for energy scavenging," *J. Sound Vib.*, vol. 292, nos. 3–5, pp. 987–998, May 2006.

[3] M. Ferrari, V. Ferrari, M. Guizzetti, D. Marioli, and A. Taroni, "Piezoelectric multifrequency energy converter for power harvesting in autonomous microsystems," *Sens. Actuators A, Phys.*, vol. 142, pp. 329–335, Mar. 2008.

[4] L. Tang and Y. Yang, "A multiple-degree-of-freedom piezoelectric energy harvesting model," *J. Intell. Mater. Syst. Struct.*, vol. 23, no. 14, pp. 1631–1647, Sep. 2012.

[5] Q. Ou, X. Chen, S. Gutschmidt, A. Wood, and N. Leigh, "A two-mass cantilever beam model for vibration energy harvesting applications," in *Proc. IEEE Int. Conf. Autom. Sci. Eng.*, Aug. 2010, pp. 6–301.

[6] P. Blanchet, "Linear vibration analysis using screw theory," Ph.D. dissertation, Dept. Mech. Eng., Georgia Inst. Technol., Atlanta, GA, USA, 1998.

[7] B. J. Dan and Y. J. Choi, "The geometrical mode and frequency analyses of a vibrating system with planes of symmetry," *J. Sound Vib.*, vol. 241, no. 5, pp. 779–795, Apr. 2001.

[8] B. J. Dan and Y. J. Choi, "Vibration analysis of single rigid-body systems having planes of symmetry," *Proc. Inst. Mech. Eng., C, J. Mech. Eng. Sci.*, vol. 216, no. 6, pp. 629–641, Jun. 2002.

[9] H. S. Kim, J. W. Kim, S.-B. Park, and Y. J. Choi, "Design of serial linkage-type vibration energy harvester with three resonant frequencies," *Smart Mater. Struct.*, vol. 26, no. 11, Nov. 2017, Art. no. 115030.

[10] H. S. Kim, W. S. Ryu, S. B. Park, and Y. J. Choi, "3-Degree-of-freedom electromagnetic vibration energy harvester with serially connected leaf hinge joints," *J. Intell. Mater. Syst. Struct.*, vol. 30, no. 2, pp. 308–322, Jan. 2019.

[11] J. Duffy, *Statics and Kinematics with Applications to Robotics*. New York, NY, USA: Cambridge Univ. Press, 1996.

[12] L. Meirovitch, *Elements of Vibration Analysis*, 2nd ed. New York, NY, USA: McGraw-Hill, 1986.

[13] M. B. Hong and Y. J. Choi, "Screw system approach to physical realization of stiffness matrix with arbitrary rank," *J. Mech. Robot.*, vol. 1, no. 2, May 2009, Art. no. 021007.

[14] M.-H. Seo, D.-H. Choi, I.-H. Kim, H.-J. Jung, and J.-B. Yoon, "Multi-resonant energy harvester exploiting high-mode resonances frequency down-shifted by a flexible body beam," *Appl. Phys. Lett.*, vol. 101, no. 12, Sep. 2012, Art. no. 123903.

[15] F. U. Khan and I. Ahmad, "Review of energy harvesters utilizing bridge vibrations," *Shock Vibrat.*, vol. 2016, pp. 1–21, Dec. 2016.

[16] S. Roundy, P. K. Wright, and J. Rabaey, "A study of low level vibrations as a power source for wireless sensor nodes," *Comput. Commun.*, vol. 26, no. 11, pp. 1131–1144, Jul. 2003.

[17] S. Qi, R. Shuttleworth, S. Olutunde Oyadiji, and J. Wright, "Design of a multiresonant beam for broadband piezoelectric energy harvesting," *Smart Mater. Struct.*, vol. 19, no. 9, Sep. 2010, Art. no. 094009.
[18] X. Bai, Y. Wen, P. Li, J. Yang, X. Peng, and X. Yue, "Multi-modal vibration energy harvesting utilizing spiral cantilever with magnetic coupling," *Sens. Actuators A, Phys.*, vol. 209, pp. 78–86, Mar. 2014.
[19] S.-B. Park, S.-J. Jang, I.-H. Kim, and Y. J. Choi, "Broadband vibration energy harvester utilizing three out-of-plane modes of one vibrating body," *Smart Mater. Struct.*, vol. 26, no. 10, Oct. 2017, Art. no. 105049.

WOOSEOK RYU is currently pursuing the Ph.D. degree in mechanical engineering with Yonsei University, Seoul, South Korea. From 2014 to 2015, he was an Intern Researcher with the Center for Robotics Research, Korea Institute of Science and Technology, South Korea. From 2015 to 2016, he was a Researcher with Hanyang University, Ansan, South Korea. His research interests are design and synthesis of robot mechanisms and vibration systems.

YEONG GEOL LEE received the B.S. degree in mechanical engineering from Yonsei University, Seoul, South Korea, in 2017, where he is currently pursuing the Ph.D. degree in mechanical engineering. His main research interests include vibration on the basis of the theory of screws, continuous vibration systems, energy harvesting, and absorbing systems.

CHUNG GEUN JEON received the B.S. degree in mechanical engineering from Yonsei University, Seoul, South Korea, in 2013, where he is currently pursuing the Ph.D. degree in mechanical engineering. His research interests are the synthesis and realization of desirable vibrational behavior of multibody systems. Applications include robotics, energy harvesting, and vibration isolation.

YONG JE CHOI received the B.S. degree from Yonsei University, Seoul, South Korea, in 1979, and the M.S. and Ph.D. degrees from the University of Florida, in 1986 and 1990, respectively, all in robotics. He is currently a Professor with the School of Mechanical Engineering, Yonsei University. His teaching and research interests include the applications of screw theory to the design of compliant robotic devices and to a new theory of vibration.